

Anonymous Referee #1

The manuscript by Wang et al. focused on the source apportionment and mixing state of black carbon in the North China Plain. The objectives of the study were to (a) determine the contributions of different sources and regions to the BC mass, (b) identify the chemical composition of BC coatings, and (c) evaluate the impacts of BC on regional radiative forcing. The authors used various methods to achieve these objectives. The major methods include a multi-wavelength optical approach combined with the source-based absorption Ångström exponent, WRF-Chem model, ART-2a, and SBDART model. The authors found that (a) the contribution of traffic emission was dominant to BC mass in the study region; (b) BC-containing particles existed in six classes to the mixing state of organic and inorganic substances; (c) the estimated BC forcing was positive with $+18.0 \text{ W m}^{-2}$ and a heating rate of 0.5 K day^{-1} in the study region. The designed experiments were comprehensive, and the results were robust. The new data generated from this study should be valuable to understand the present status of the regional air quality and radiative forcing affected by BC in the North China Plain under the background of emission reduction. Therefore, I would suggest the manuscript for publication after the authors address the following specific comments.

Response: The authors thank the reviewer's valuable suggestions, and we believe that the revised manuscript has been significantly improved after considering the comments. Below are the point-to-point responses, and the modifications to the manuscript are marked in the revised manuscript.

(1) Although a photoacoustic instrument was used to correct the impact of filter matrix scattering of AE33 aethalometer, the PAX was operated at a single wavelength of 532 nm, which may bring uncertainty for other wavelengths of AE33 absorption. This should be pointed out in the study.

Response: We agree with the reviewer. In the revised manuscript, we added a sentence to address the this uncertainty. It now reads as follows:

“As shown in Fig. S2, a 520 nm wavelength of AE33 absorption was strongly

correlated with the PAX absorption ($R^2 = 0.97$, $p < 0.01$). The slope of 2.57 was then used to correct the AE33 data. However, a single-wavelength-based correction method may result in underestimation at $\lambda = 370$ and 470 nm, and overestimation at $\lambda = 590$, 660 , and 880 nm (Kim et al., 2019).”

(2) A Nafion dryer was used for ACSM. How about the AE33, PAX, and SPAMS? High ambient humidity can also influence the measurements of these instruments. A schematic of the measurement system should be used to show the setup of each instrument.

Response: The collected ambient aerosols were dried before measurements by all instruments. We followed the reviewer’s suggestion and added a schematic of the instrumental setups. Please see Figure R1 below (also see Figure S1 in the revised supplemental material).

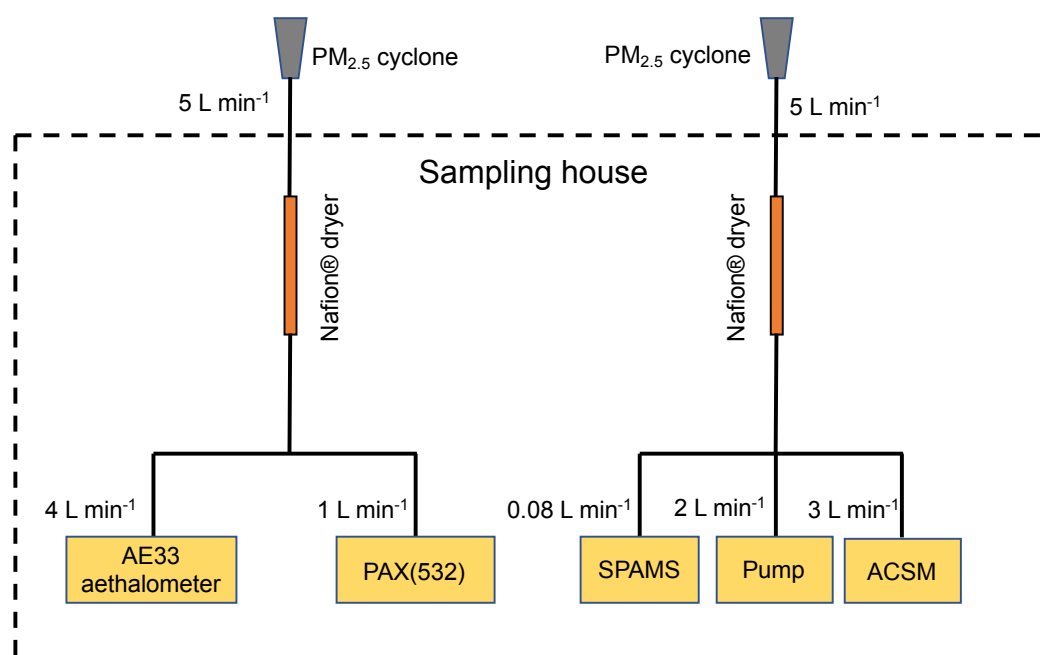


Figure R1. Schematic presentation of the instrumental setups of the ambient aerosol measurements.

(3) The authors should provide more information on bench tests, as the vehicle emission is a crucial component of the BC sources; relevant references should be cited.

Response: Following the reviewer's suggestion, we added more description about the bench tests in the revised manuscript. It now reads as follows:

“The motor vehicle exhaust emissions were performed using a LDWJ6/135 detection system of loading and speed reduction on the light duty diesel vehicle (Shenzhen Huiyin Industrial Development Co., Ltd, Shenzhen, China). This system contains two different sizes of expansion cylinders that are used to carry the driving wheels of the vehicles. Fig. S5 shows the schematic presentation of the instrumental setup of motor vehicle exhaust emissions. Gasoline and diesel cars at idle and at different driving speeds (i.e., 20 and 40 km h⁻¹) were tested. The automobile exhaust smoke particles were collected using a particle sampling probe in the exhaust pipe. The particles were dried by a silica gel dryer before AE33 aethalometer measurement. The measured $b_{\text{abs}}(\lambda)$ used to estimate the AAE was averaged over the period that the driving speed was relatively stable.”

(4) Insufficient detail is given regarding the radiative forcing calculations. The radiative forcing is related to the vertical information of the atmosphere. The authors used the OPAC model to retrieve the vertical optical parameters used in the SBDART model, but the brief description makes the calculation unclear. More information about the OPAC model should be added in the supporting information.

Response: Following the reviewer's suggestion, we added more description of the OPAC model in the revised supplemental material (Text S3). It reads as follows:

“The aerosol optical depth (AOD), single scattering albedo (SSA), and asymmetric parameter (AP) are important parameters used in the SBDART model to estimate aerosol radiative effect. In this study, these optical parameters were derived by the OPAC model. A detailed description of the software package of OPAC has been documented by Hess et al. (1998). The measured mass concentrations of OC, EC, and water-soluble ions as well as the estimated mineral dust ($= [\text{Fe}]/0.035$) were input in the OPAC model to estimate the AOD, SSA, and AP. The measurements of these chemical species are described in Text

S1. The number concentration of BC in the OPAC model was constrained by the measured EC mass concentration. Although several water-soluble ions and mineral dust were obtained, they did not cover all water-soluble and insoluble materials. Therefore, the number concentrations of water-soluble and insoluble materials were tuned for OPAC model based on the measured data. This was done by comparing the OPAC-derived light scattering, light absorption, and SSA with the corresponding PAX-measured ones until the differences were within 5% for each parameter. After the aerosol light extinction coefficient (sum of light scattering and absorption) was obtained, the AOD was then estimated as follows (Hess et al., 1998):

$$\text{AOD} = \sum_j \int_{H_{j,\min}}^{H_{j,\max}} \sigma_{e,j}(h) dh = \sum_j \sigma_{e,j}^1 N_j(0) \int_{H_{j,\min}}^{H_{j,\max}} e^{-\frac{h}{Z_j}} dh \quad (\text{S1})$$

where $H_{j,\max}$ and $H_{j,\min}$ were the upper and lower boundary in layer j ; $\sigma_{e,j}$ was the surface aerosol light extinction coefficient in layer j ; h was the layer height; $\sigma_{e,j}^1$ represented the aerosol light extinction coefficient that was normalized to 1 particle cm^{-3} ; N_j was the number concentration in layer j ; and Z was the scale height. The OPAC-derived AODs were tuned to match the satellite-derived AODs (<https://giovanni.gsfc.nasa.gov/giovanni>) by altering the scale height in OPAC until the difference between them was within 5%. Owing to the closure with AOD and anchoring of the chemical composition, the assumptions in the OPAC model did not exhibit a significant impact on the estimation of radiative effect using SBDART model (Satheesh and Srinivasan 2006).”

(5) One finding of this study is the change of BC source in winter NCP through comparison with previous studies in this region. The authors considered this as a successful example of coal-to-gas switching to reduce pollutants under the new regulations by the Chinese State Council released in 2013. It would be useful to see a thorough comparison between the results of this study and those conducted before 2013 in this region. There should be relevant data from previous measurements by

others in this region.

Response: Following the reviewer’s suggestion, we added BC source apportionment studies conducted before 2013 in the NCP region. This information was updated in Figure 4 in the revised manuscript (also see Figure R2 below).

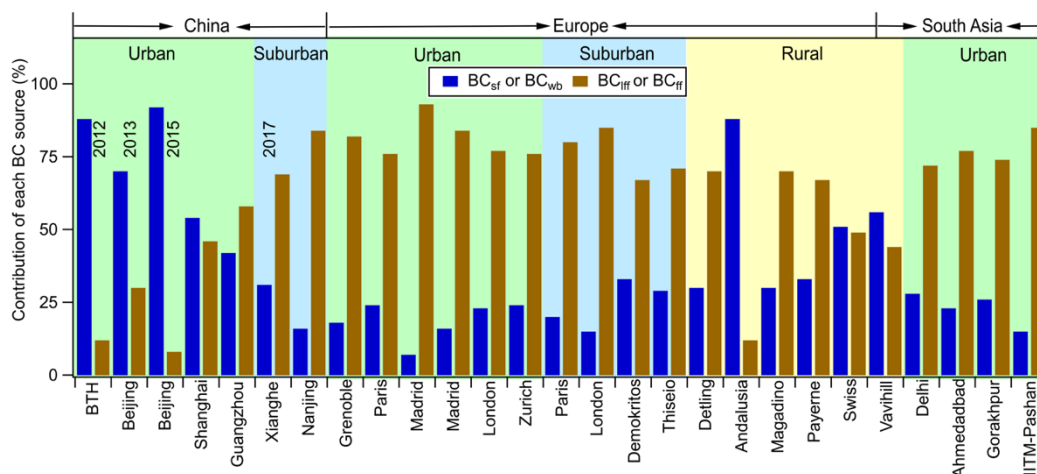


Figure R2. Comparisons of the different sources of black carbon (BC) in urban, suburban, and rural areas in China and Europe. BC_{sf} and BC_{wb} describe BC from solid fuel sources and wood burning, respectively. BC_{lff} and BC_{ff} represent BC from liquid fossil fuel and solid fossil fuel sources, respectively. Detailed information of the data is summarized in Table S1.

(6) The term ‘Aethalometer model’ gets misused in places. This refers to the data analysis technique, not the instrument itself.

Response: To make it clearer, we changed the “Aethalometer model” to “multi-wavelength optical method” in the revised manuscript.

(7) The map of Fig. S6 does not make much sense to someone unfamiliar with Chinese geography. Suggest showing a zoomed-out version showing the wider region.

Response: Following the reviewer’s suggestion, we modified the map of Fig. S6 in the revised manuscript. Please see Figure R3 below (also see Figure S8 in the revised supplemental material).

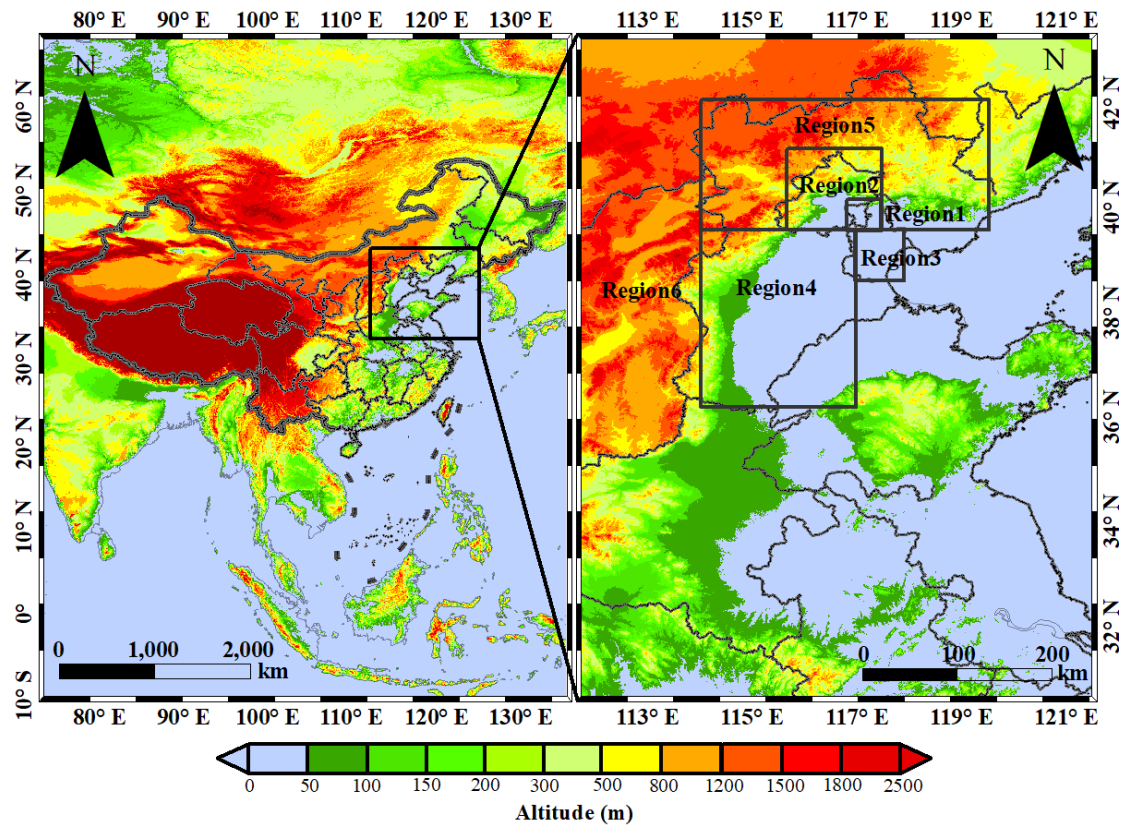


Figure R3. Division of different regions in the Weather Research and Forecasting model coupled with chemistry (WRF-Chem).

(8). *The authors may improve the manuscript content by avoiding grammar and spelling errors throughout the text. I'm not going to list them, but the manuscript should be checked carefully and polished by a native English speaker.*

Response: The revised manuscript was polished by an English language editing agency.

Anonymous Referee #2

Summary:

This paper discusses measurements of black carbon (BC) made with an AE33 aethalometer and a SP-AMS in the North China Plain (NCP) during winter in 2017-2018. These observations are discussed in the context of recent emission reduction policies. Initial laboratory experiments were made of different fuel sources in an environmental chamber to develop a model to interpret the aethalometer measurements. This model was then applied to 2 months of measurements at a ground site, and the results are interpreted in the context of WRF-Chem modeling results to estimate relative contributions from regional sources and the BC radiative effect. The relative contributions of liquid fossil fuel sources and solid fuel sources were evaluated, and these relative sources were discussed in the context of their contribution to the regional BC radiative effect.

The observations and the analysis presented here are a valuable contribution to the literature, given the importance of BC as a climate forcer and the NCP as a significant anthropogenic source region for these aerosols. The conclusion that focusing on a reduction of BC from solid fuel sources could lead to greater gains than liquid fuels is an important conclusion for policy makers.

While it's clear that a significant amount of work went into the acquisition of measurements and the analysis of results presented in this study, the discussion is often challenging to follow. While each separate part of the measurements, analysis, and modeling were described in Section 2, it is often not clear which measurement or model contributed to the results discussed in Section 3. The paper would also benefit from a more clear discussion of the BC observations in light of best practices for discussing observations from different instruments established in the recent literature. In addition, the radiative forcing calculation is not clearly described.

Response: The authors appreciate the reviewer's valuable suggestions, and we believe that the revised manuscript has been significantly improved after addressing the comments. Below are the point-to-point responses, and the modifications to the

manuscript are marked.

General Comments:

(1) Observations of BC with the different instruments used in the study should be more clearly distinguished (eBC, rBC) as discussed in Lack et al. 2014. This is an important issue when comparing observations between different instruments, as BC is operationally defined, and this point should be made clearly in the discussion. This is particularly confusing in the discussion of the source-specific AAE model, as it seems both observations from the aethalometer and the SP-AMS are used to determine the source-specific AAE values.

Response: We followed the reviewer's suggestion and clarified the term of BC measured by different instruments. According to the review studies of BC by Lack et al. (2014) and Petzold et al. (2013), we used "equivalent BC (eBC)" for AE33 aethalometer measurements and "elemental carbon (EC)-containing particles" for SPAMS measurements. The source-specific AAE was calculated based on the aerosol light absorption which was measured by AE33 aethalometer. We have clarified this in the revised manuscript. It now reads as follows:

"Table 1 summarizes the average AAEs obtained from the sources of liquid fossil fuels and solid fuels. These source-specific AAEs were calculated using $b_{\text{abs}}(370)$ and $b_{\text{abs}}(880)$ (Eqs. 3 and 4)."

(2) It is also important in the context of the BC radiative effect calculation, as observations of BC mass loadings can differ by a factor of 2 or more when comparing different measurement techniques.

Response: We agree with the reviewer that different BC instruments induce uncertainties in BC measurements in studies. In the revised manuscript, we clarified this point, and it reads as follows:

"Compared to previous DRE obtained from the SBDART model, the atmospheric DRE derived by eBC values in this study ($+18.0 \pm 9.6 \text{ W m}^{-2}$) was

comparable to that of South China (+17.0 W m⁻², Huang et al., 2011) but was lower than that of Northwest China (+16.6 to +108.8 W m⁻², Zhao et al., 2019). In addition to the varying BC burden in different areas, the BC measurement techniques used in different studies may also contribute to the differences in BC DRE calculations.”

(3) The discussion of the radiative forcing is not very clear, and I had a hard time following how this calculation was performed. More details need to be given. In addition, this appears to be a calculation of the BC radiative effect (rather than radiative forcing), as described in Heald et al. 2014.

Response: After carefully read the study of Heald et al. (2014), we changed the original used ‘radiative forcing’ to ‘radiative effect’ in the revised manuscript. Additionally, we added more detailed description about the calculation of BC radiative effect. It now reads as follows:

“Aerosol direct radiative effect (DRE) (Heald et al. 2014) at the top of the atmosphere (TOA) or at the Earth’s surface (ES) is the difference between the incoming (\downarrow) and outgoing (\uparrow) solar fluxes (F) with and without aerosols:

$$\text{DRE} = (F \downarrow - F \uparrow)_{\text{with aerosol}} - (F \downarrow - F \uparrow)_{\text{without aerosol}} \quad (8)$$

The aerosol DRE in the atmosphere was calculated by subtracting the DRE at the Earths’ surface from the DRE at the top of the atmosphere.

In this study, the Santa Barbara DISORT Atmospheric Radiative Transfer (SBDART) model that was developed by Ricchiazzi et al. (1998) was used to perform the radiative transfer calculations in the shortwave spectral region of 0.25–4.0 μm . The SBDART model is a widely used tool for estimating aerosol DRE in the atmosphere (e.g., Zhang et al., 2017; Rajesh and Ramachandran, 2018; Boiyo et al., 2019). A detailed description of this model can be found in Ricchiazzi et al. (1998). The aerosols’ optical depth, single scattering albedo, and asymmetric parameters are essential input factors in the SBDART model. These

optical parameters were estimated using the Optical Properties of Aerosols and Clouds (OPAC) model (Hess et al., 1998). Detailed calculations are shown in Text S3. Moreover, the surface albedo, solar zenith angle, and atmospheric parameter profiles are also important input factors in the SBDART model. The surface albedo was derived from the Moderate Resolution Imaging Spectroradiometer (<https://modis-atmos.gsfc.nasa.gov/ALBEDO/index.html>, last access: November 2019). The solar zenith angle was estimated using the latitude, longitude, and sampling time of the location. The atmospheric vertical profiles (including vertical distributions of temperature, pressure, water vapor, and ozone density) of mid-latitude winter embedded in the SBDART model were used.”

(4) Overall, the paper could benefit from English language editing.

Response: The revised manuscript was polished by an English language editing agency.

Specific Comments:

(5) The title is quite long.

Response: We shortened the title as follows:

“Measurement report: Source and mixing state of black carbon aerosol in the North China Plain: Implications for radiative effect”

(6) Page 1, lines 23-25. It is unclear here how the “local emissions” differ from the “emissions in the NCP”. If this is meant to differentiate local emissions relative to regional emissions this could be more clearly stated.

Response: Yes, it means to differentiate local emissions from regional emissions. To make it clearer, we revised this sentence in the manuscript. It now reads as follows:

“The air quality model indicated that local emissions were the dominant contributors to eBC at the measurement site. However, regional emissions from NCP were a critical factor for high eBC pollution.”

(7) A schematic of the instrument setup during the environmental chamber experiments and the measurement campaign could be a helpful addition. Additionally the map showing the location of the measurement site (S1) would be helpful in the main text.

Response: Following the reviewer's suggestion, we have added the schematic of instrumental setups of our ambient measurements (see Figure R1 below and Figure S1) and source experiments (see Figure R2 below and Figure S4) in the revised supplementary material. Moreover, map of the sampling location was put in the main text (see Figure 1 in the revised main text).

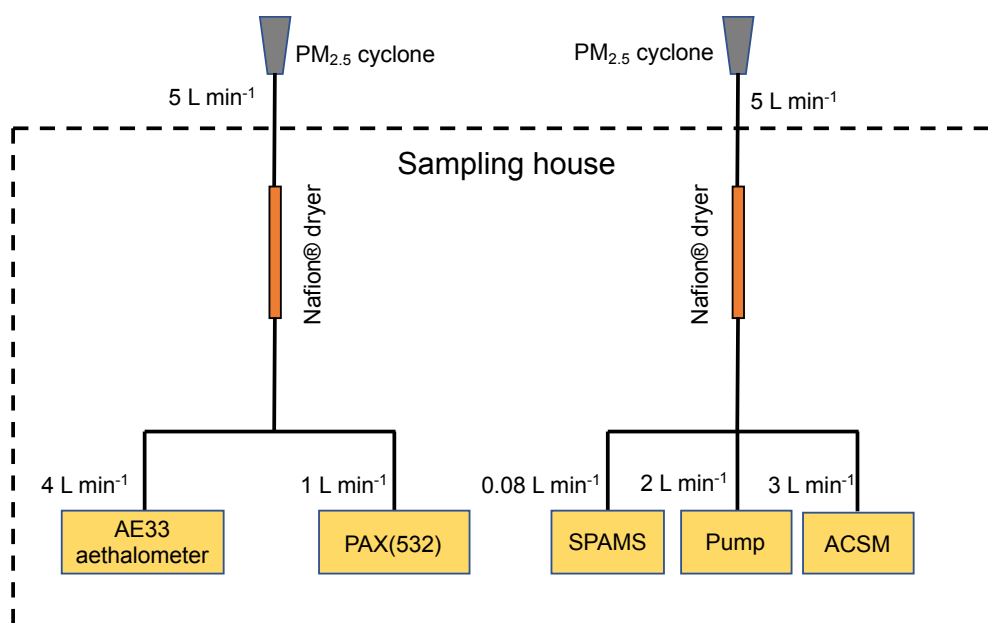


Figure R1. Schematic presentation of the instrumental setups of the ambient aerosol measurements.

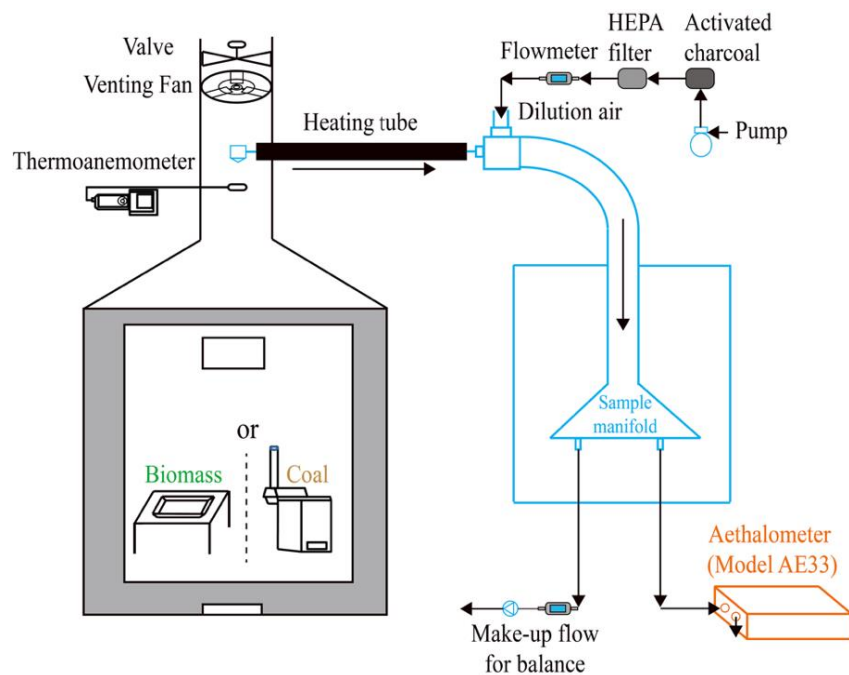


Figure R2. Schematic presentation of the instrumental setups of source experiments of biomass burning and coal combustion.

(8) *Some more details would be useful for the observations from the source emission experiments in order that these could be more easily compared with other similar experiments. At what point during the burns was the emitted smoke measured?*

Response: We thank the reviewer’s insightful suggestion. In the revised manuscript, we added more description of the source emission experiments, which includes the information concerned by the reviewer. It now reads as follows:

“A custom-made passivated aluminum chamber ($\sim 8 \text{ m}^3$) was used to characterize the emission of solid fuels (i.e., biomass and coal) (Fig. S4). Performance evaluation of this chamber was done by Tian et al. (2015). Several types of biomass residues (wheat straw, rice straw, and corn stalk, cotton stalk, sesame stalk, soybean straw, and firewood) and coal (bituminous coal and honeycomb briquet) were used to represent biomass burning and coal combustion that occurs in the NCP. Each weighted sample was burned on a platform or in a stove that was placed inside the combustion chamber. For

biomass burning, the chamber background $b_{\text{abs}}(\lambda)$ was measured by AE33 aethalometer before ignition. When the background $b_{\text{abs}}(\lambda)$ was close to zero and stable, a propane torch was used to ignite the biomass on the platform. For coal combustion, a burned-out honeycomb coal in the stove was used as the igniter after the background $b_{\text{abs}}(\lambda)$ was small and stable in the chamber. The emitted smokes of each burn test were first diluted by a Model 18 dilution sampler (Baldwin Environmental Inc., Reno, NV, USA) before AE33 aethalometer measurements (Fig. S4). The $b_{\text{abs}}(\lambda)$ used to estimate the AAE was averaged over the entire period of each burn from ignition to $b_{\text{abs}}(\lambda)$ back to the background.

The motor vehicle exhaust emissions were performed using a LDWJ6/135 detection system of loading and speed reduction on the light duty diesel vehicle (Shenzhen Huiyin Industrial Development Co., Ltd, Shenzhen, China). This system contains two different sizes of expansion cylinders that are used to carry the driving wheels of the vehicles. Fig. S5 shows the schematic presentation of the instrumental setup of motor vehicle exhaust emissions. Gasoline and diesel cars at idle and at different driving speeds (i.e., 20 and 40 km h⁻¹) were tested. The automobile exhaust smoke particles were collected using a particle sampling probe in the exhaust pipe. The particles were dried by a silica gel dryer before AE33 aethalometer measurement. The measured $b_{\text{abs}}(\lambda)$ used to estimate the AAE was averaged over the period that the driving speed was relatively stable.”

(9) Do the values in Table 1 represent average values of the aerosol optical properties during the entire period of the burn? What does the “test number” in Table 1 refer to? Is this the number of experiments performed? This should be made clear in the caption.

Response: Yes, the aerosol optical properties in Table 1 were calculated using the average light absorption of the entire period of each burn. The test number denotes the number of performed experiments. We added notes in the revised Table 1 (also see Table R1 below).

Table 1. Summary of aerosol absorption Ångström exponent (AAE) obtained from source experiment.

	Solid fuel				Liquid fuel	
	Crop residues	Firewood	Bituminous coal	Honeycomb briquet	Gasoline	Diesel
Maximum	3.3	3.2	1.4	5.2	1.5	1.3
Minimum	1.6	2.7	1.0	2.2	1.4	1.0
Average ^a	2.4	2.9	1.1	4.0	1.5	1.2
S.D. ^b	0.4	0.2	0.2	0.9	0.1	0.1
Test number ^c	30	4	4	16	3	7

^aThe average value was calculated using the light absorption of the entire period of each burn.

^bS.D. represents standard deviation.

^cTest number denotes the number of performed experiments.

(10) I found the discussion in 3.1.1 and Figure 1 to be unclear. Given the range of values for AAE for the different fuel types shown in Table 1, the limitations of the aethalometer model, which assumes a single value for AAE for liquid fuels and solid fuels, should be more clearly discussed in the text.

Response: From the computational equations, the limitation of ‘aethalometer model’ is mainly from the applied source-specific AAE. Due to the high variation in the solid fuel AAE (e.g., 1.1–4.0 in this study), the selection of different value in the ‘aethalometer model’ can cause uncertainties in estimation of contribution from each source (e.g., solid fuels and liquid fuels) to total BC mass. Most of the current studies used source-specific AAEs from previous publication (e.g., Healy et al., 2017; Rajesh and Ramachandran, 2018; Zheng et al., 2019). Some other studies obtained the source-specific AAE through comparison with results from external source apportionment methods, such as ACSM-based organic aerosol (OA) sources (Ealo et al., 2016) and ¹⁴C technique (Martinsson et al., 2017; Zotter et al., 2017). In this study, we conducted the source experiments to obtain the possible suitable source-specific AAEs. In addition, we performed sensitivity analyses by comparing results of BC source apportionment with different OA sources (i.e., HOA and BBOA+CCOA) to verify the rationality of the applied AAE values. In the revised manuscript, we added

the limitation of the ‘aethalometer model’. And based on the comment from Reviewer 1, we changed the term “Aethalometer model” to “multi-wavelength optical method” in the revised manuscript. It now reads as follows:

“From Eqs. 1–4 of the multi-wavelength optical method, its limitation is attributed to the choice of source-specific AAE. Since AAE exhibited high variations (e.g., 1.1–4.0 in this study), different AAE selections may lead to uncertainties when estimating the contributions of solid fuels and liquid fuels to eBC mass. In this study, the obtained average AAE_{lf} (1.3) and AAE_{sf} (2.8) were applied in the multi-wavelength optical method to obtain eBC source apportionment. A sensitivity test for each eBC source and organic aerosol (OA) subtype was further performed to verify the rationality of the used AAEs.”

References:

Ealo, M., Alastuey, A., Ripoll, A., Pérez, N., Minguillón, M. C., Querol, X. and Pandolfi, M.: Detection of Saharan dust and biomass burning events using near-real-time intensive aerosol optical properties in the north-western Mediterranean, *Atmos. Chem. Phys.*, 16(19), 12567–12586, <https://doi.org/10.5194/acp-16-12567-2016>, 2016.

Healy, R. M., Sofowote, U., Su, Y., Deboisz, J., Noble, M., Jeong, C.-H., Wang, J. M., Hilker, N., Evans, G. J., Doerksen, G., Jones, K. and Munoz, A.: Ambient measurements and source apportionment of fossil fuel and biomass burning black carbon in Ontario, *Atmos. Environ.*, 161, 34–47, <https://doi.org/10.1016/j.atmosenv.2017.04.034>, 2017.

Martinsson, J., Abdul Azeem, H., Sporre, M. K., Bergström, R., Ahlberg, E., Öström, E., Kristensson, A., Swietlicki, E. and Eriksson Stenström, K.: Carbonaceous aerosol source apportionment using the Aethalometer model – evaluation by radiocarbon and levoglucosan analysis at a rural background site in southern Sweden, *Atmos. Chem. Phys.*, 17(6), 4265–4281, <https://doi.org/10.5194/acp-17-4265-2017>, 2017.

Rajesh, T. A. and Ramachandran, S.: Black carbon aerosols over urban and high altitude remote regions: Characteristics and radiative implications, *Atmos.*

Environ., 194, 110–122, <https://doi.org/10.1016/j.atmosenv.2018.09.023>, 2018.

Zheng, H., Kong, S., Wu, F., Cheng, Y., Niu, Z., Zheng, S., Yang, G., Yao, L., Yan, Q., Wu, J., Zheng, M., Chen, N., Xu, K., Yan, Y., Liu, D., Zhao, D., Zhao, T., Bai, Y., Li, S. and Qi, S.: Intra-regional transport of black carbon between the south edge of the North China Plain and central China during winter haze episodes, *Atmos. Chem. Phys.*, 19(7), 4499–4516, <https://doi.org/10.5194/acp-19-4499-2019>, 2019.

Zotter, P., Herich, H., Gysel, M., El-Haddad, I., Zhang, Y., Močnik, G., Hüglin, C., Baltensperger, U., Szidat, S. and Prévôt, A. S. H.: Evaluation of the absorption Ångström exponents for traffic and wood burning in the Aethalometer-based source apportionment using radiocarbon measurements of ambient aerosol, *Atmos. Chem. Phys.*, 17(6), 4229–4249, <https://doi.org/10.5194/acp-17-4229-2017>, 2017.

(11) Does Table 2 give observations from the SP-AMS? As this discusses the number of particles, that would seem to be the case but this should be clearly stated (e.g. by referring to rBC rather than BC).

Response: Yes, Table 2 shows the observations from SPAMS. As replied in comment (1) above, the ‘BC’ in table was revised to ‘EC’ as shown in Table R2 (also see Table 2 in the revised manuscript).

Table R2. Summary of names, numbers, and fractions of six types of elemental carbon (EC)-containing particles determined by a single particle aerosol mass spectrometer.

Group	Number of particles	Fraction of particles (%)
EC internally mixed with OC and sulphate (EC-OCsO _x)	235874	51.9
EC internally mixed with Na and K (EC-NaK)	107272	23.6
EC internally mixed with K, sulphate, and nitrate (EC-KSO _x NO _x)	75227	16.6
EC from biomass burning (EC-BB)	26307	5.8
Pure-EC	5083	1.1
Unidentified EC (EC-others)	4670	1
Total EC-containing	454433	100

(12) Page 11, lines 13. How was this percent contribution determined? Is this from the WRF-Chem model or does this use the observed BC? Is the BC concentration shown in Figure 5 from the model results or from the observations?

Response: The percent contributions of local emissions and regional transport were obtained from WRF-Chem model. The BC concentration shown in Figure 5 was the observation values. We clarified in the manuscript, and it now reads as follows:

“As shown in Fig. S8, six source regions were identified in the WRF-Chem model to quantify the contributions of local emissions and regional transport to observed eBC mass. The information on each source region is summarized in Table S2, and their contributions to observed eBC mass are shown in Fig. 5.”

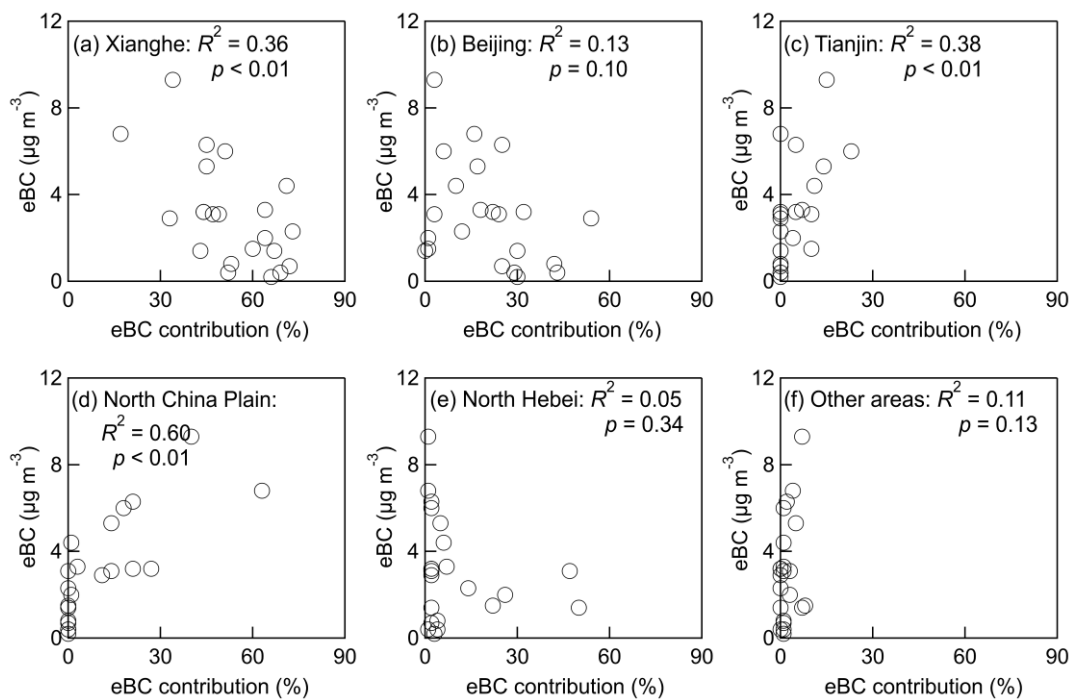


Figure R3. Scatter plots of the measured mass concentrations of equivalent black carbon (eBC) versus the eBC contributions of different source regions obtained by WRF-Chem model.

(13) Figure 6. It would be useful to replace the Region 1-6 labels shown in the figure with the names of the regions used in the text (or include this information in the caption).

Response: Following the reviewer's suggestion, we added this information in the figure caption. Please see the Figure R4 below (also see Figure 7 in the revised manuscript).

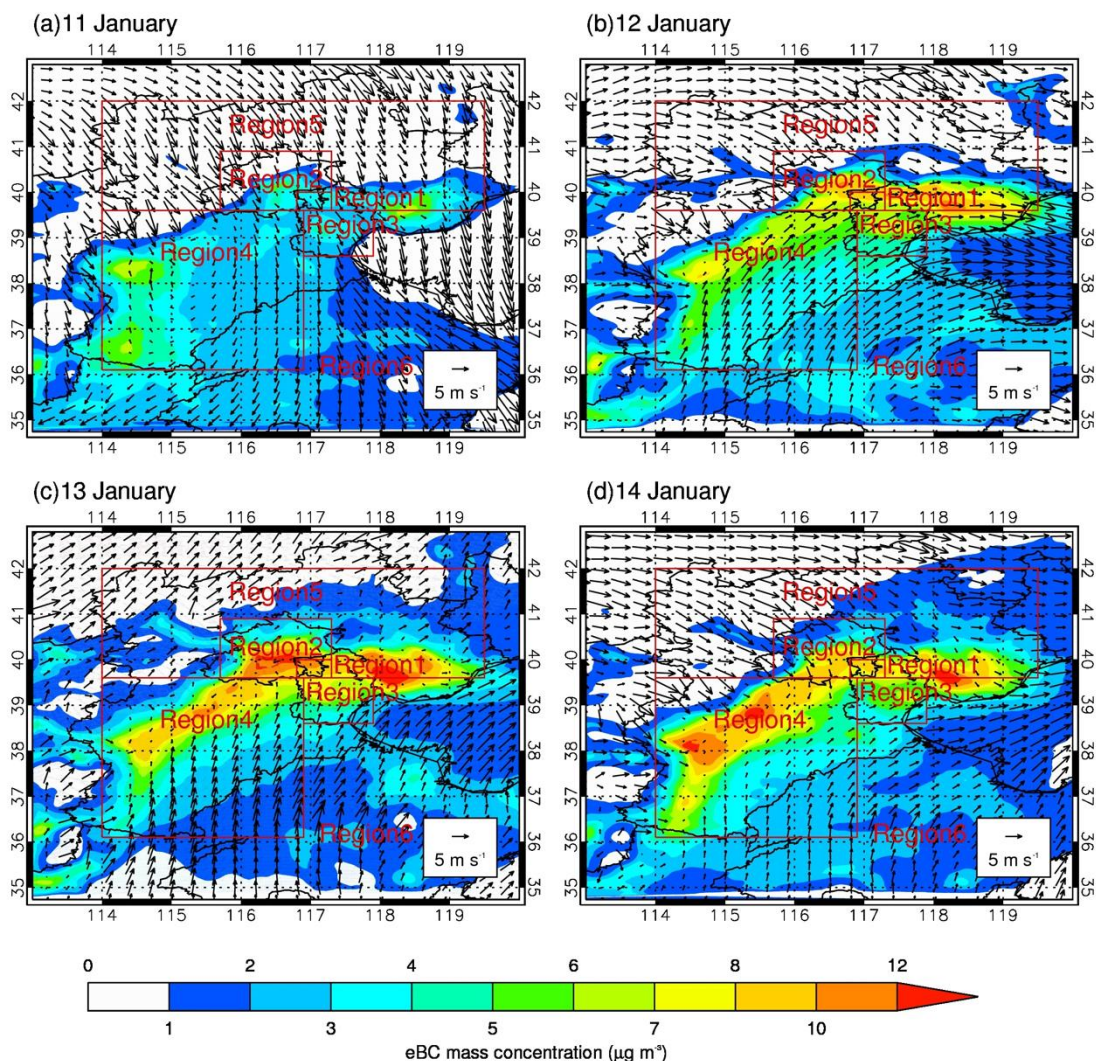


Figure R4. Distributions of the daily average mass concentrations of equivalent black carbon (eBC) ($\mu\text{g m}^{-3}$, represented by the color bar) at Xianghe and surrounding areas from 11th to 14th January, 2018 simulated by WRF-Chem model. The arrow denotes the wind speed. The red rectangles represent different source regions, which Region 1 is Xianghe, Region 2 is Beijing, Region 3 is Tianjin, Region 4 is North China Plain, Region 5 is North Hebei Province, and Region 6 is other areas except Region 1–5.

(14) Figure 8. It is unclear what the percentile range on the x-axis refers to. Is this with respect to the BC mass loading?

Response: Yes, the percentile range is the BC mass loading of different sources. We revised this figure to make it clearer. Please see Figure R5 below (also see Figure 9 in the revised manuscript).

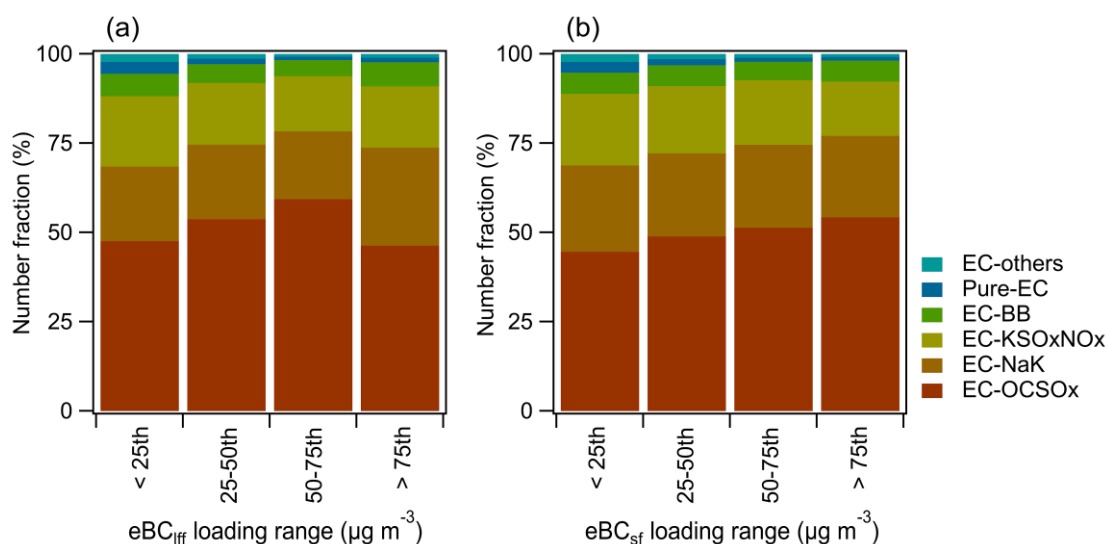


Figure R5. Number fractions of elemental carbon (EC)-containing particle classes at different loading ranges of equivalent black carbon (eBC) from sources of (a) liquid fossil fuels (eBC_{lff}) and (b) solid fuels (BC_{sf}). The 25th, 50th, and 75th denote the 25%, 50%, and 75% percentiles, respectively.

(15) It would be useful to discuss the results in Section 3.3 in the context of the different BC source emissions discussed in Section 3.1

Response: We thank the reviewer’s suggestion. As shown in Figure R5 above, we actually discussed the characteristics of chemical composition of EC-containing particles in the context of the different eBC sources in the original manuscript. We revised the manuscript in this part to make the discussion clearer. It now reads as follows:

“Fig. 9 shows the number of fractions of each class of EC-containing particles at different ranges of eBC_{lff} and eBC_{sf}. The EC-OCSOx number fraction increased as eBC_{sf} increased. In contrast, it dropped when eBC_{lff} was higher than the value of the 75th percentile of BC_{lff}. This indicated a greater impact of solid fuel source on EC-OCSOx at a high eBC loading environment compared to the liquid fossil fuel source.”

“The number fraction of EC-NaK increased with an increase in BC_{lff} but kept stable with BC_{sf} as shown in Fig. 9. These results demonstrate that EC-NaK was

likely associated with fresh traffic emissions than from solid fuels.”

(16) Are the results in Section 3.4 from the WRF-Chem model? It is not clearly stated in the text.

Response: The results of radiative effect in Section 3.4 were estimated from the SBDART model. We added a sentence at the beginning of this paragraph to clarify this in the revised manuscript:

“Fig. 11 shows the eBC DRE variations as estimated by the SBDART model.”

(17) Also it would be useful to provide some context for this estimation of the BC radiative effect in terms of previous calculations in the literature for the NCP region.

Response: We followed the reviewer’s suggestion and added some comparisons of BC radiative effect from previous studies. It now reads as follows:

“In contrast, eBC exhibited a DRE range of +0.6 to +20.8 W m⁻² with an average of +4.4 ± 3.0 W m⁻² at the TOA, indicating a net energy gain and warm effect. This was attributed to the strong BC light absorption property that can impede the back scattered radiation reaching the TOA. The eBC DRE at the TOA in this study was comparable to the value over the NCP region (+6 to +8 W m⁻², Li et al., 2016).”

“Compared to previous DRE obtained from the SBDART model, the atmospheric DRE derived by eBC values in this study (+18.0 ± 9.6 W m⁻²) was comparable to that of South China (+17.0 W m⁻², Huang et al., 2011) but was lower than that of Northwest China (+16.6 to +108.8 W m⁻², Zhao et al., 2019).”

References:

Heald, C.L., Ridley, D.A., Kroll, J.H., Barrett, S.R.H., Cady-Pereira, K.E., Alvarado, M.J. and Holmes, C.D., 2014. Contrasting the direct radiative effect and direct radiative forcing of aerosols.

Lack, D.A., Moosmüller, H., McMeeking, G.R., Chakrabarty, R.K. and Baumgardner, D., 2014. Characterizing elemental, equivalent black, and refractory black carbon

aerosol particles: a review of techniques, their limitations and uncertainties. Analytical and bioanalytical chemistry, 406(1), pp.99-122.

Response: We thank the reviewer providing relevant references, and we have added them in the revised manuscript.

Measurement report: Sources and mixing state of black carbon aerosol in the North China Plain: Implications for radiative effect

Qiyuan Wang^{1,2}, Li Li¹, Jiamao Zhou¹, Jianhuai Ye³, Wenting Dai¹, Huikun Liu¹, Yong Zhang¹, Renjian Zhang^{4,5}, Jie Tian¹, Yang Chen⁶, Yunfei Wu⁴, Weikang Ran¹, and Junji Cao^{1,2}

¹Key Laboratory of Aerosol Chemistry and Physics, State Key Laboratory of Loess and Quaternary Geology, Institute of Earth Environment, Chinese Academy of Sciences, Xi'an 710061, China

²CAS Center for Excellence in Quaternary Science and Global Change, Xi'an 710061, China

³School of Engineering and Applied Sciences, Harvard University, Cambridge, MA 02138, USA

⁴Key Laboratory of Middle Atmosphere and Global Environment Observation, Institute of Atmospheric Physics, Chinese Academy of Sciences, Beijing 100029, China

⁵Xianghe Observatory of Whole Atmosphere, Institute of Atmospheric Physics, Chinese Academy of Sciences, Xianghe 065400, China

⁶Chongqing Institute of Green and Intelligent Technology, Chinese Academy of Sciences, Chongqing 400714, China

Correspondence to: Qiyuan Wang (wangqy@ieecas.cn) and Junji Cao (cao@loess.llqg.ac.cn)

Abstract. Establishment of the sources and mixing state of black carbon (BC) aerosol is essential for assessing its impact on air quality and climatic effects. A winter campaign (December 2017–January 2018) was performed in the North China Plain (NCP) to evaluate the sources, coating composition, and radiative effects of BC under the background of emission reduction. Results showed that the sources of liquid fossil fuels (i.e., traffic emissions) and solid fuels (i.e., biomass and coal burning) contributed 69% and 31% to the total equivalent BC (eBC) mass, respectively. These values were arrived at by using a combination of multi-wavelength optical approach with the source-based aerosol absorption Ångström exponent values. The air quality model indicated that local emissions were the dominant contributors to eBC at the measurement site. However, regional emissions from NCP were a critical factor for high eBC pollution. A single particle aerosol mass spectrometer identified six classes of elemental carbon (EC)-containing particles. They included: EC coated by organic carbon and sulphate (52% of total EC-containing particles), EC coated by Na and K (24%), EC coated by K, sulphate, and nitrate (17%), EC associated with biomass burning (6%), pure-EC (1%), and others (1%). Different BC sources exhibited distinct impacts on the EC-containing particles. A radiative transfer model showed that the amount of detected eBC can produce an atmospheric direct radiative effect of +18.0 W m⁻² and a heating rate of 0.5 K day⁻¹. This study shows

删除了: Evaluation of s...ources and mixing state of black carbon aerosol under the background of emission reduction ...n the North China Plain: li

删除了: Regional Climate-Environment Research for Temperate East Asia

删除了: County, Hebei Province,

删除了: Accurate understanding ...f the sources and mixing state of black carbon (BC) aerosol is essential for assessing its impacts ...on air quality and climatic effects. Here, a ... winter campaign (December 2017 ... anuary 2018) was conducted ...erformed in the North China Plain (NCP) to evaluate the sources, coating composition, and radiative effects of BC under the background of emission reduction since 2013... Results showed that the sources of liquid fossil fuel source... (i.e., traffic emissions) and solid fuel source... (i.e., biomass and coal burning) contributed 69% and 31% the total equivalent BC (eBC) mass, respectively. These values were arrived at by... using a combination of multi-wavelength optical approach combined ...ith the source-based aerosol absorption Ångström exponent values. The air quality model indicated...that local emissions was ...ere the dominant contributors to eBC at the measurement site on average... Hh...however, regional emissions in ...romthe...NCP exerted ...ere a critical role ...actor for high eBC episode...ollution. A single particle aerosol mass spectrometer identified sS...x classes of elemental carbon (EC)BC...containing particles were identified... They included:ing... (1) ...B... coated by organic carbon and sulphate (52% of total EB...-containing particles), (2) ...B... coated by Na and K (24%), (3) ...B... coated by K, sulphate, and nitrate (17%), (4) B...C associated with biomass burning (6%), (5) P...ure-EB... (1%), and (6) ...thers (1%). Different BC sources exhibitedhad... distinct impacts on those ...he EB...-containing particles. A radiative transfer model estimated ...howed that the amount of detected eBC detected ...an produce an atmospheric direct radiative effectforcing

that reductions of solid fuel combustion-related BC may be an effective way of mitigating regional warming in the NCP.

删除了: Results presented herein highlight that further reductions of solid fuel combustion-related BC may be an more effective way to mitigate regional warming in the NCP, although larger BC contribution was from liquid fossil fuel source

1 Introduction

In the few past decades, black carbon (BC) aerosol has attracted considerable attention due to its substantial effects on the climate and atmospheric environment (Bond et al., 2013). It has strong light-absorption abilities that lead to substantive climate changes in the global atmosphere (+1.1 W m⁻²). It is considered to be the second largest anthropogenic warming agent after carbon dioxide (Bond et al., 2013).

In addition, the high atmospheric BC loading inhibits the development of a planetary boundary layer and enhances haze pollution (Ding et al., 2016). Reducing atmospheric BC loading is regarded as a win-win intervention for mitigating climate change and improving air quality (Kopp and Mauzerall, 2010).

删除了: Over the few past decades, black carbon (BC) aerosol has attracted considerable attention due to its substantial effects on the climate and atmospheric environment (Bond et al., 2013). It has BC can affect climate via direct or semidirect radiative effects or indirect cloud-albedo effects (Boucher et al., 2013). Due to its strong light-absorption abilities that lead to, BC can produce a substantial climate forcing changes globally in the present-day global atmosphere (+1.1 W m⁻²), and hence it is considered as to be the second largest anthropogenic warming agent after carbon dioxide (Bond et al., 2013). Moreover, the high atmospheric BC loading can depress the development of a planetary boundary layer and aggravate enhances haze pollution (Ding et al., 2016). Due to the short atmospheric residence time, reducing atmospheric BC loading is regarded as a win-win policy intervention to mitigate climate change and improves...

Different emission sources (e.g., fossil fuel and biomass burning) and complex physicochemical properties (e.g., morphology, size, and coating composition) have hindered the efforts to assess the climatic and environmental impacts of BC (Vignati et al., 2010). To determine BC sources, current methods rely on data obtained from offline filter-based or online spectroscopic techniques (Briggs and Long, 2016). Among them, the carbon isotope approach (Zhang et al., 2015) and multi-wavelength optical method (Zotter et al., 2017) are often used to determine BC sources. The carbon isotope approach can be used to obtain relatively accurate results of BC sources. However, the analysis is limited by time resolution of the filter samples. The multi-wavelength optical method utilizes online data and has the advantage of a superior time resolution when determining BC sources. The principle of the multi-wavelength optical method is based on Beer-Lambert's Law. It utilizes measured aerosol light absorption at different wavelengths (Sandradewi et al., 2008). However, due to the lack of source-specific aerosol absorption Ångström exponent (AAE), studies often cite AAEs from previous literatures with fuel types being distinct among studies (Kalogridis et al., 2018; Zheng et al., 2019). These components induce potential uncertainties in using the multi-wavelength optical method. Therefore, a diverse set of AAEs from different source emissions are needed to improve the performance of this method.

删除了: Owing to BC's various different emission sources (e.g., fossil fuel and biomass burning) and complex physicochemical properties (e.g., morphology, size, and coating composition) have hindered the efforts to, large uncertainty still remains in assessing their climatic and environmental impacts of BC (Vignati et al., 2010). To determine For BC source apportionment, current methods rely on data obtained from the data obtained from offline filter-based or online spectroscopic techniques (Briggs and Long, 2016). Among them, the carbon isotope approach (e.g., $\Delta^{13}C$, Zhang et al., 2015) and multi-wavelength optical method (e.g., aethalometer model Zotter et al., 2017) are often used to quantify determine BC the sources of BC (e.g., Zotter et al., 2017; Zhang et al., 2015). The carbon isotope approach could be used to obtain relatively accurate results of BC source apportionment. However, the analysis is limited by time resolution of the filter samples. The multi-wavelength optical method aethalometer model which utilizes online data and has the advantage of a superior time resolution when determining BC sources. The principle of the multi-wavelength optical method aethalometer model is based on the Beer-Lambert's Law. It utilizes using measured aerosol light absorption at different wavelengths (Sandradewi et al., 2008). However, due to the lack of source-specific aerosol absorption Ångström exponent (AAE), a number of studies often adopted cite AAEs in aethalometer model cited from previous literatures even the fuel types are being distinct among studies (e.g., Kalogridis et al., 2018; Zheng et al., 2019). These components may induce a large potential uncertainties in using the multi-wavelength optical method the accuracy of BC source apportionment. Therefore, a diverse set of AAEs from different source emissions are needed to improve the performance of the aethalometer model

Black carbon mixing state is whereby another chemical composition is coated on BC particles (internally mixed) or exists as separate particles (externally mixed). Freshly emitted BC particles (e.g., diesel vehicle

删除了: As an important chemical property of aerosol, BC mixing state describes whether it is whereby another other chemical composition is coated on BC particles (internally mixed) or exists as separate particles (externally mixed). Generally, f

emission) exhibit typical external mixing, but over time, they become internally mixed with other non-BC materials (e.g., organics, sulphate, and nitrate) during atmospheric processes (Eriksson et al., 2017). Compared to uncoated BC particles, the coated ones enhance the absorption efficiency of solar radiation by a factor of 1.2–2.0. This factor is strongly correlated with the chemical composition of the coatings on BC particles and their thickness (Wang et al., 2014; Fierce et al., 2016; Liu et al., 2017). Determination of BC mixing states through observation is challenging. Advances in online mass spectrometric techniques have enabled the elucidation of chemical characteristics of BC coatings. Based on this method, studies have reported direct observations of chemical compositions associated with BC-containing particles and their evolutionary features in the atmosphere (Zhang et al., 2014; Arndt et al., 2017).

删除了: gradually ...internally mixed with other non-BC materials (e.g., organics, sulphate, and nitrate) during atmospheric processes (Eriksson et al., 2017). Compared with ...o uncoated BC particles, the coated ones can ...hance the absorption efficiency of solar radiation by a factor of 1.20,... which ...his factor is strongly associated ...orrelated with the chemical composition of the coatings on BC particles and their thickness (Wang et al., 2014; Fierce et al., 2016; Liu et al., 2017). Although d...etermining...tion of BC mixing states through observations...is still ...hallenging,...emerging a...dvances in online mass spectrometry...techniques have enabled make it possible for obtaining ...he elucidation of chemical characteristics of BC coatings. Based on this method, some ...udies have reported direct observations of chemical compositions associated with BC-containing particles as well as...nd their evolutionary features in the atmosphere (e.g.,

China is a hotspot for anthropogenic BC emissions. It accounts for up to 14% of the global BC radiative forcing (Li et al., 2016). In the past decade, China has experienced severe air pollution, especially in the North China Plain (NCP) (An et al., 2019). To improve air quality, the Chinese State Council has promulgated a series of regulations to reduce air pollutants. The most rigorous regulation of the 'Action Plan for the Prevention and Control of Air Pollution (APPCAP)' released on 10th September 2013, aimed

删除了: As ... hotspot region ...or anthropogenic BC emissions. It, China...accounts for up to 14% of the global BC radiative forcing (Li et al., 2016). Over ...n the past decade, China has suffered from...xperienced severe serious...air pollution, especially in the North China Plain (NCP) (An et al., 2019). To improve air quality, the Chinese State Council has been ...romulgated a series of regulations to reduce air pollutants., e.g.,...Tt...e most rigorous regulation of the 'Action Plan for the Prevention and Control of Air Pollution'

at reducing particulate matter by up to 10% in 2017 relative to 2012 levels for all prefecture-level cities in China. Studies have demonstrated the effectiveness of China's clean air policies in the reduction of particulate matter (Zhang et al., 2019). Decreased BC and co-emitted pollutant levels affects the interactions between BC and secondary aerosols which in turn results in changes in the physicochemical properties of BC aerosol. To reduce emissions, the assessment of physicochemical characteristics of BC will enhance the understanding of anthropogenic climate impact in China. However, studies focused on this aspect are limited. Therefore, we performed intensive measurements during winter in the last year of the APPCAP at a regional site in the NCP region to determine the influences of different sources and regions to BC loading, identify the chemical composition of BC coatings, and evaluate the impact of BC on radiative effect.

删除了: which ...imed...to ...t reducing... particulate matter by up to 10% by ...n 2017 relative to 2012 levels for all prefecture-level cities in China. Previous s...udies have demonstrated the effectiveness of China's clean air actions ...olicies in the reduction of particulate matter (Zhang et al., 2019). The d...ecreased BC and co-emitted pollutant levels can...affects the interactions between BC and secondary aerosols which in turn results in changes in the physicochemical properties of BC aerosol. In the context of...o reduce emissions reduction... the assessment of physicochemical characteristics of BC will be useful for improving our...hance the understanding of anthropogenic climate impacts...in current ...hina. However, studies focused on this aspect are limited at present... Therefore, we conducted ...erformed intensive measurements during winter in the last year of the APPCAP at a regional site in the NCP region to (1)...determine the contributions ...nfluences of different sources and regions to BC mass ...oading, (2)...identify the chemical composition of BC coatings, and (3)...evaluate the impacts

设置了格式: 上标

2 Methodology

2.1 Sampling site

The sampling site was the Xianghe Atmospheric Integrated Observatory (39°45' N, 116°57' E). It is located in a small county of Xianghe, north of the NCP (Fig. 1). The county has an area of 458 km² and a total population of 0.36 million. It is bordered by Beijing in the northwest (~45 km) and Tianjin in the southeast (~79 km). This place is considered to be a regional observatory site that is exposed to frequent pollution plumes (e.g., urban, rural, or mixed origins) from surrounding areas (Wang et al., 2019a). Intensive measurements were performed in winter (1st December, 2017 to 31st January, 2018). During this period, atmospheric temperature was -1°C while relative humidity was 35%.

2.2 Field Observations

2.2.1 Aethalometer measurement

A model AE33 aethalometer (Magee Scientific, Berkeley, CA, USA) was used to measure the aerosol light absorption at multi-wavelengths ($b_{\text{abs}}(\lambda)$, $\lambda = 370, 470, 520, 590, 660, 880, \text{ and } 950 \text{ nm}$) with a PM_{2.5} cyclone (SCC 1.829, BGI Inc. USA). A schematic representation of the instrumental setup of the ambient aerosol measurements is shown in Fig. S1. The operational principle of this instrument was described in detail by Drinovec et al. (2015). Briefly, seven different light sources are used to irradiate the filter deposition spot, and light attenuation is detected by optical sensors. The biases associated with the nonlinear loading effect were resolved by the AE33 aethalometer. However, the impact of filter matrix scatters interferes with the accuracy of measurements (Drinovec et al., 2015). To overcome this limitation, a photoacoustic extinctions (PAX) operating at a $\lambda = 532 \text{ nm}$ was installed in parallel with AE33 aethalometer. A detailed operating principle and calibrating procedures of PAX were described in our previous publication (Wang et al., 2018a). As shown in Fig. S2, a 520 nm wavelength of AE33 absorption was strongly correlated with the PAX absorption ($R^2 = 0.97, p < 0.01$). The slope of 2.57 was then used to correct the AE33 data. However, a single-wavelength-based correction method may result in underestimation at $\lambda = 370$ and 470 nm, and overestimation at $\lambda = 590, 660, \text{ and } 880 \text{ nm}$ (Kim et al., 2019).

删除了: the

删除了: S

删除了: ion

删除了: which

删除了: suffers from

删除了: conducted

删除了: from

Furthermore, based on the assumption that only BC is absorbed at the near-infrared region, the mass concentration of equivalent BC (eBC) was estimated using $b_{\text{abs}}(880)$. The mass absorption cross section (MAC) of eBC at $\lambda = 880$ nm ($\text{MAC}_{\text{eBC}}(880)$) was a conversion factor between $b_{\text{abs}}(880)$ and eBC. It was retrieved from the correlation between $b_{\text{abs}}(880)$ and filter-based elemental carbon (EC, see Text S1). A good correlation of $b_{\text{abs}}(880)$ and EC mass concentration ($R^2 = 0.86, p < 0.01$) was observed as shown in Fig. S3. Therefore, the $\text{MAC}_{\text{eBC}}(880)$ was estimated by $b_{\text{abs}}(880)$ dividing the EC mass concentration ($\text{MAC}_{\text{eBC}}(880) = b_{\text{abs}}(880)/[\text{EC}]$).

2.2.2 Single particle aerosol mass spectrometer (SPAMS)

A SPAMS (Hexin Analytical Instrument Co., Ltd., Guangzhou, China) was used to determine the real-time chemical composition of EC-containing particles. Ambient aerosol was drawn into the evacuated system through a critical orifice (100 μm) at a flowrate of 0.08 L min^{-1} . After passing through an aerodynamic lens, the sampled particles were accelerated to certain speeds. Two diode Nd:YAG lasers (MLL-III-532, Changchun, China) operating at 532 nm were used to determine the aerodynamic diameters (0.2–2.0 μm) of the passing particles. A pulsed 266 nm Nd:YAG laser (UL728F11-F115, Quantel, France) was then used to ionize the particles. Finally, a dual-polarity time-of-flight mass spectrometer was applied to detect the generated positive and negative fragment ions. A MATLAB-based YAADA toolkit (www.yaada.org) was used to search and analyze the imported single-particle mass spectral data. An adaptive resonance theory-based neural network algorithm (ART-2a) was used to perform particle clustering, with a vigilance factor of 0.8, a learning rate of 0.05, and 20 iterations (Li et al., 2019).

2.3 Source emission experiments

A custom-made passivated aluminum chamber (~ 8 m^3) was used to characterize the emissions of solid fuels (i.e., biomass and coal) (Fig. S4). Performance evaluation of this chamber was done by Tian et al. (2015). Several types of biomass residues (wheat straw, rice straw, corn stalk, cotton stalk, sesame stalk, soybean straw, and firewood) and coal (bituminous coal and honeycomb briquet) were used to represent biomass burning and coal combustion that occurs in the NCP. Each weighted sample was burned on a

删除了:
删除了: Measurement of BC mixing state
移动了(插入) [1]
删除了: (
删除了: ,
删除了: The chemical composition of BC coatings
删除了: d by a
删除了: single particle aerosol mass spectrometer
上移了 [1]: (SPAMS, Hexin Analytical Instrument Co., Ltd., Guangzhou, China)
删除了: The a
删除了: is
删除了: via
删除了: with
删除了: ;
删除了: a
删除了: are
删除了: ed
删除了: are
删除了:
删除了:
删除了: fter then, a
删除了: is
删除了: os
删除了: is
删除了: os
删除了: utilized
删除了: which
删除了: set
删除了: 2.2.3 Measurement of organic aerosol
删除了: The emitted smokes were diluted by a Model 18 dilution
删除了: is given in
删除了: of alimentary crops
删除了: e.g.,
删除了: and
删除了:), economic crops (e.g.
删除了: and
删除了:)
删除了: the
删除了: red

platform or a stove that was placed inside the combustion chamber. For biomass burning, the chamber background $b_{\text{abs}}(\lambda)$ was measured by AE33 aethalometer before ignition. When the background $b_{\text{abs}}(\lambda)$ was close to zero and stable, a propane torch was used to ignite the biomass on the platform. For coal combustion, a burned-out honeycomb coal in the stove was used as the igniter after the background $b_{\text{abs}}(\lambda)$ was small and stable in the chamber. The emitted smokes of each burn test were first diluted by a Model 18 dilution sampler (Baldwin Environmental Inc., Reno, NV, USA) before AE33 aethalometer measurements (Fig. S4). The $b_{\text{abs}}(\lambda)$ used to estimate the AAE was averaged over the entire period of each burn from ignition to $b_{\text{abs}}(\lambda)$ back to the background.

The motor vehicle exhaust emissions were performed using a LDWJ6/135 detection system of loading and speed reduction on the light duty diesel vehicle (Shenzhen Huiyin Industrial Development Co., Ltd. Shenzhen, China). This system contains two different sizes of expansion cylinders that are used to carry the driving wheels of the vehicles. Fig. S5 shows the schematic presentation of the instrumental setup of motor vehicle exhaust emissions. Gasoline and diesel cars at idle speed and at different driving speeds (i.e., 20 and 40 km h⁻¹) were tested. The automobile exhaust smoke particles were collected using a particle sampling probe in the exhaust pipe. The particles were dried by a silica gel dryer before AE33 aethalometer measurement. The measured $b_{\text{abs}}(\lambda)$ used to estimate the AAE was averaged over the period that the driving speed was relatively stable.

2.4 Data analysis methods

2.4.1 Multi-wavelength optical method

A multi-wavelength optical method proposed by Sandradewi et al. (2008) was used to quantify the influence of liquid fossil fuels (i.e., gasoline and diesel for traffic emissions) and solid fuels (i.e., biomass and coal) to α_{BC} mass at Xianghe. The measured $b_{\text{abs}}(\lambda)$ at the wavelengths of 370 nm ($b_{\text{abs}}(370)$) and 880 nm ($b_{\text{abs}}(880)$) were used in this study. The $b_{\text{abs}}(\lambda)$ value is determined by carbonaceous aerosols and mineral dust. The mass fraction of mineral dust in PM_{2.5} was small (11%) during the campaign. Moreover, the MAC of mineral dust was 0.09 m² g⁻¹ at $\lambda = 370$ nm and 0.001 m² g⁻¹ at $\lambda = 880$ nm (Yang et al., 2009). Therefore, the light absorption capacity of mineral dust in this study is negligible. For carbonaceous absorption, it can be divided into light absorption attributed to primary emissions (i.e., BC

删除了: (Wang et al., 2018b)

删除了: Meanwhile, bituminous coal and honeycomb briquet that commonly used in the NCP were collected in Shanxi and Shaanxi Provinces. A typical stove that extensively used in the NCP was applied for coal test burns inside the combustion chamber (Tian et al., 2019). Furthermore, motor vehicle exhaust emissions were conducted using bench tests.

删除了: several

删除了: Aethalometer model

删除了: An aethalometer model

删除了: applied

删除了: contributions

删除了: the model

删除了: As demonstrated previously,

删除了: can be contributed

删除了: Due to the small

删除了: (11% of PM_{2.5} mass)

删除了: and its small mass absorption cross section

删除了: (

删除了: ,

删除了: ,

删除了: caused by

删除了: can be neglected

删除了: Previous studies have demonstrated that the $b_{\text{abs}}(880)$ is mainly contributed by BC aerosol, while $b_{\text{abs}}(370)$ is associated with BC, primary and secondary brown carbon

and primary brown carbon (BrC) and secondary formation (i.e., secondary BrC) (Laskin et al., 2015).

Therefore, the $b_{\text{abs}}(370)$ and $b_{\text{abs}}(880)$ could be calculated from the perspective of emission sources as follows:

$$b_{\text{abs}}(880)_{\text{lff}} + b_{\text{abs}}(880)_{\text{sf}} = b_{\text{abs}}(880) \quad (1)$$

$$b_{\text{abs}}(370)_{\text{lff}} + b_{\text{abs}}(370)_{\text{sf}} = b_{\text{abs}}(370) - b_{\text{abs}}(370)_{\text{sBrC}} \quad (2)$$

$$\frac{b_{\text{abs}}(370)_{\text{lff}}}{b_{\text{abs}}(880)_{\text{lff}}} = \left(\frac{370}{880}\right)^{-\text{AAE}_{\text{lff}}} \quad (3)$$

$$\frac{b_{\text{abs}}(370)_{\text{sf}}}{b_{\text{abs}}(880)_{\text{sf}}} = \left(\frac{370}{880}\right)^{-\text{AAE}_{\text{sf}}} \quad (4)$$

where $b_{\text{abs}}(880)_{\text{lff}}$ and $b_{\text{abs}}(880)_{\text{sf}}$ refer to the light absorptive capacity of BC at $\lambda = 880$ nm from liquid fossil fuel and solid fuel sources, respectively; $b_{\text{abs}}(370)_{\text{lff}}$ and $b_{\text{abs}}(370)_{\text{sf}}$ are the light absorptive capacities of BC and primary BrC at $\lambda = 370$ nm emitted from liquid fossil fuel and solid fuel sources, respectively; $b_{\text{abs}}(370)_{\text{sBrC}}$ is the absorption caused by secondary BrC, which was estimated by a BC-tracer method combined with a minimum R -squared approach (Wang et al., 2019b); and AAE_{lff} and AAE_{sf} described the aerosol AAEs from sources of liquid fossil fuels and solid fuels, respectively.

After obtaining $b_{\text{abs}}(880)_{\text{lff}}$ and $b_{\text{abs}}(880)_{\text{sf}}$, the mass concentrations of eBC contributed by liquid fossil fuel and solid fuel sources (eBC_{lff} and eBC_{sf} , respectively) were calculated by dividing $\text{MAC}_{\text{eBC}}(880)$ as follows:

$$\text{eBC}_{\text{lff}} = \frac{b_{\text{abs}}(880)_{\text{lff}}}{\text{MAC}_{\text{eBC}}(880)} \quad (5)$$

$$\text{eBC}_{\text{sf}} = \frac{b_{\text{abs}}(880)_{\text{sf}}}{\text{MAC}_{\text{eBC}}(880)} \quad (6)$$

The underlying assumption of Eqs. (5) and (6) was that the $\text{MAC}_{\text{eBC}}(880)$ value was the same from liquid fossil fuel and solid fuel sources. The rationality of this assumption has been confirmed by Zotter et al. (2017).

2.4.2 Regional chemical dynamical model

In this study, local and regional contributions to eBC mass at Xianghe were quantified by the Weather Research and Forecasting model coupled with Chemistry (WRF-Chem). The eBC utilized as a tracer was

删除了: (pBrC and sBrC, respectively)

删除了: Finally

删除了: can

删除了: absorption

删除了: derived

删除了: represent

删除了: absorption

删除了: p

删除了: representative of the BrC

删除了: formation processes

删除了: sources

删除了: then

删除了: the mass absorption cross section of BC at $\lambda = 880$ nm (

设置了格式: 下标

删除了:)

设置了格式: 下标

删除了: as those

删除了: , which is justified

删除了: Due to a strong correlation between $b_{\text{abs}}(880)$ and EC mass concentration ($R^2 = 0.86$, $p < 0.01$, Fig. S3), the daily $\text{MAC}_{\text{BC}}(880)$ can be estimated by daily $b_{\text{abs}}(880)$ dividing by the corresponding EC mass concentration.

删除了: The

删除了: versus

删除了: was

删除了: Here

删除了: used

added into the WRF-Chem to improve the model's operational efficiency (Zhao et al., 2015). Detailed descriptions regarding the model's configurations are shown in Text S2. The performance of WRF-Chem simulation was evaluated with a mathematical parameter of index of agreement (IOA). This index describes the relative differences between the simulated and observed values. The IOA values vary from 0 to 1. An index that is closer to 1 is associated with better performance of the simulation model. The IOA was calculated as follows (Li et al., 2011):

$$IOA = 1 - \frac{\sum_{i=1}^N (S_i - O_i)^2}{\sum_{i=1}^N (|S_i - S_{ave}| + |O_i - O_{ave}|)^2} \quad (7)$$

where S_i and O_i were the simulated and observed mass concentrations of eBC, respectively; S_{ave} and O_{ave} represented the average value of simulated and observed eBC loadings, respectively; while N denoted the number of simulations.

2.4.3 Radiative effect and heating rate

Aerosol direct radiative effect (DRE) (Heald et al., 2014) at the top of the atmosphere (TOA) or at the Earth's surface (ES) is the difference between the incoming (\downarrow) and outgoing (\uparrow) solar fluxes (F) with and without aerosols:

$$DRE = (F \downarrow - F \uparrow)_{\text{with aerosol}} - (F \downarrow - F \uparrow)_{\text{without aerosol}} \quad (8)$$

The aerosol DRE in the atmosphere was calculated by subtracting the DRE at the Earth's surface from the DRE at the top of the atmosphere.

In this study, the Santa Barbara DISORT Atmospheric Radiative Transfer (SBDART) model that was developed by Ricchiazzi et al. (1998) was used to perform the radiative transfer calculations in the shortwave spectral region of 0.25–4.0 μm . The SBDART model is a widely used tool for estimating aerosol DRE in the atmosphere (e.g., Zhang et al., 2017; Rajesh and Ramachandran, 2018; Boiyo et al., 2019). A detailed description of this model can be found in Ricchiazzi et al. (1998). The aerosols' optical depth, single scattering albedo, and asymmetric parameters are essential input factors in the SBDART model. These optical parameters were estimated using the Optical Properties of Aerosols and Clouds (OPAC) model (Hess et al., 1998). Detailed calculations are shown in Text S3. Moreover, the surface albedo, solar zenith angle, and atmospheric parameter profiles are also important input factors in the SBDART model. The surface albedo was derived from the Moderate Resolution Imaging

删除了: More d

删除了: l

删除了: , which

删除了: can

删除了: , with the value

删除了: meaning the

删除了: simulation

删除了: is

删除了: are

删除了: loadings

删除了: and

删除了: s

删除了: Estimations of r

删除了: forcing

删除了: A

删除了: (

删除了:

删除了:

删除了:)

删除了: the

删除了: direct radiative forcing (

删除了: F) by

删除了: ic science community

删除了: Raju et al., 2016; Singh et al., 2016;

删除了: The

删除了: principle

删除了: SBDART

Spectroradiometer (<https://modis-atmos.gsfc.nasa.gov/ALBEDO/index.html>, last access: November 2019). The solar zenith angle was estimated using the latitude, longitude, and sampling time of the location. The atmospheric vertical profiles (including vertical distributions of temperature, pressure, water vapor, and ozone density) of mid-latitude winter embedded in the SBDART model were used.

5 After obtaining eBC DRE, the atmospheric heating rate ($\frac{\partial T}{\partial t}$, in unit of K d⁻¹) induced by eBC was further calculated using the first law of thermodynamics and hydrostatic equilibrium as follows (Liou, 2002):

$$\frac{\partial T}{\partial t} = \frac{g}{C_p} \times \frac{\Delta F}{\Delta P} \quad (8)$$

where $\frac{g}{C_p}$ described the lapse rate, of which g was the acceleration due to gravity and C_p represented the specific heat capacity of air at a constant pressure (1006 J kg⁻¹ K⁻¹); ΔF was the atmospheric forcing induced by the eBC aerosol; while ΔP was representative of the atmospheric pressure difference, which was assumed to be 300 hPa.

3 Results and discussion

3.1 BC source apportionment

3.1.1 Determination of source-specific AAEs

15 Table 1 summarizes the average AAEs obtained from the sources of liquid fossil fuels and solid fuels. These source-specific AAEs were calculated using $b_{\text{abs}}(370)$ and $b_{\text{abs}}(880)$ (Eqs. 3 and 4). The average AAE_{eff} was 1.3 ± 0.2, with the gasoline car exhibiting higher values (1.4 – 1.5) compared to the diesel engine car (1.1 – 1.2). In comparison with AAE_{eff}, a higher average value was exhibited by AAE_{sf} (2.8 ± 1.0). The highest value was, however, obtained from honeycomb briquet emissions (4.0 ± 0.9), followed
20 by burning firewood (2.9 ± 0.2), crop residues emissions (2.4 ± 0.4), and bituminous coal emissions (1.1 ± 0.2). The variance in AAE_{sf} were attributed to the different types of solid fuels and their burning conditions. For example, the AAE_{sf} exhibited a weak but significant inverse correlation with combustion efficiency at 95% confidence interval as shown in Fig. S6 ($R^2 = 0.14$, $p < 0.05$).

From Eqs. 1–4 of the multi-wavelength optical method, its limitation is attributed to the choice of source-specific AAE. Since AAE exhibited high variations (e.g., 1.1–4.0 in this study), different AAE selections

删除了: The DRFs induced by BC alone (or total aerosol) at the Earth's surface (ES), the top of the atmosphere (TOA), and in the atmosphere were estimated by the difference in the net flux with and without BC (or aerosol) under cloud-free conditions.

删除了: The optical properties of aerosol optical depth (AOD), single scattering albedo (SSA), and asymmetric parameter (ASP) are essential input parameters in the SBDART model, and they were determined by an Optical Properties of Aerosol and Cloud (OPAC) model (Hess et al., 1998). The measured BC and water-soluble inorganic ions as well as the estimated water-soluble organic matter (assuming that the water-soluble organic matter accounts for 49% of organic matter based on the result of Zhang et al., 2018) and water insoluble matter (calculated by the mass concentration of PM_{2.5} minus BC and water-soluble matter) were used as input parameters in OPAC to reconstruct the AOD, SSA, and ASP. The difference between the reconstructed SSA by OPAC and measured SSA by PAX was 1.4%, indicating a reasonable reconstruction result. Further

删除了: s

删除了: is

删除了: s

删除了: is

删除了: and

删除了: is

删除了: shows

删除了: characteristics of

删除了: experiments

删除了: ,

删除了: higher values for

删除了: than those for

删除了: Compared

删除了: larger

删除了: found

删除了: for

删除了: with t

删除了: largest

删除了: one

删除了: burning

删除了: large variabilities

删除了: potentially

删除了: affected by the various

删除了: ;

删除了: f

删除了: shows

删除了: , Fig. S4

may lead to uncertainties when estimating the contributions of solid fuels and liquid fuels to eBC mass. In this study, the obtained average AAE_{lff} (1.3) and AAE_{sf} (2.8) were applied in the multi-wavelength optical method to obtain eBC source apportionment. A sensitivity test for each eBC source and organic aerosol (OA) subtype was further performed to verify the rationality of the used AAEs. The mass concentration of OA was measured using an aerosol chemical speciation monitor (ACSM). The primary OA was further resolved into hydrocarbon-like OA (HOA), biomass burning OA (BBOA), and coal combustion OA (CCOA). HOA is associated with liquid fuel sources while the BBOA and CCOA are associated with solid fuel sources. Detailed descriptions of OA measurements and its source apportionment are shown in the supplementary material of Wang et al. (2019b).

In light of the range of source-based AAEs as shown in Table 1, a series of AAE_{lff} and AAE_{sf} were used to obtain the mass concentrations of eBC_{lff} and eBC_{sf} . Correlations for eBC_{lff} versus HOA and eBC_{sf} versus (BBOA + CCOA) were then established as shown in Fig. 2. AAE_{lff} variations could not affect the correlations between eBC_{lff} and HOA at a fixed AAE_{sf} . However, their R^2 increased as AAE_{sf} increased before 3. When the AAE_{sf} was larger than 3, the R^2 was constant regardless of the variability in AAE_{sf} .

In contrast, at a fixed AAE_{lff} , the R^2 between eBC_{sf} and (BBOA + CCOA) was independent of the AAE_{sf} variation. For the AAE_{lff} (1.3) and AAE_{sf} (2.8) used in this study, the coefficients of determining eBC_{lff} versus HOA ($R^2 = 0.60$) and eBC_{sf} versus (BBOA + CCOA) ($R^2 = 0.66$) were belonged to the upper limit of all the R^2 values obtained from different ranges of AAE_{lff} and AAE_{sf} (Fig. 2). Furthermore, the estimated ratios of HOA/ eBC_{lff} (1.7) and (BBOA + CCOA)/ eBC_{sf} (8.4) were comparable to the values calculated with emission factors (Cheng et al., 2010; Sun et al., 2018). Therefore, the AAE_{lff} of 1.3 and AAE_{sf} of 2.8 were reasonable selections for this study.

3.1.2 Characteristics of eBC_{lff} and eBC_{sf}

Fig. 3a shows that the hourly eBC mass concentration varied from 0.1 to 24.4 $\mu\text{g m}^{-3}$ with an average of $3.6 \pm 4.0 \mu\text{g m}^{-3}$. The estimated eBC_{lff} ($2.5 \mu\text{g m}^{-3}$) comprised 69% of the total eBC loading, which was over two times larger than the contribution of eBC_{sf} (31%, $1.1 \mu\text{g m}^{-3}$) (Fig. 3b). This indicated that at Xianghe, traffic emissions were the dominant contributors to eBC mass. As shown in Fig. 3c, the diurnal variation of eBC_{lff} exhibited peaks at 08:00 and 19:00. These findings coincided with the rush-hour traffic

- 删除了: T
- 删除了: aethalometer model
- 删除了: the
- 删除了: The OA subtypes contributed by liquid fossil fuel (i.e., HOA) and solid fuel sources (i.e., BBOA + CCOA) were used to verify the reliability of model results.
- 删除了:
- 删除了: the
- 删除了: put into the aethalometer model
- 删除了: The c
- 删除了: were then established
- 删除了: (
- 删除了: 1)
- 删除了: The variations in
- 删除了: can
- 删除了: ,
- 删除了: but
- 删除了: ;
- 删除了: after
- 删除了: kept
- 删除了: used
- 删除了: ation of
- 删除了: 1
- 删除了: Based on the BC source apportionment result
- 删除了: are
- 删除了: os
- 删除了: pair of
- 删除了: is
- 删除了: a
- 删除了: T
- 删除了: average
- 删除了: was
- 删除了: and varied largely from 0.1 to 24.4 $\mu\text{g m}^{-3}$ during the campaign (Fig. 2a)
- 删除了: ($2.5 \mu\text{g m}^{-3}$)
- 删除了: 2
- 删除了: s
- 删除了: at Xianghe
- 删除了: 2
- 删除了: two
- 删除了: , which were

of the morning and evenings. The peaks of eBC_{sf} were also found to be in the same period as eBC_{lf} . However, they could be attributed to residential cooking in surrounding rural areas, where solid fuels are a commonly used source of household energy (Liu et al., 2016). Due to the increased planetary boundary layer height and wind speed (data sources see Text S1), decreased eBC_{lf} and eBC_{sf} values were observed in the afternoon (Fig. 3d). In contrast to the rapid decline in eBC_{lf} after 19:00, eBC_{sf} persisted at a high level until midnight. Moreover, the eBC_{sf} fraction in eBC was also elevated towards the night, indicating enhanced heating activities using solid fuels during cold nights.

Fig. 4 compares findings from various studies regarding eBC sources, and their detailed information is summarized in Table S1. Because of the heavy traffic, liquid fossil fuel emissions are major contributors to eBC mass in urban areas. However, emissions from solid fuels contribute more to eBC mass compared to liquid fossil fuels in rural area. This is attributed to wood burning used as an energy source in rural households. In addition, the dominant eBC source in winter NCP has changed from past solid fuels to current liquid fossil fuels. This change is probably attributed to the rigorous regulations that have been promulgated by the Chinese State Council in recent years. The large-scale project of coal-to-gas switching is considered an effective way of reducing atmospheric pollutants (Qin et al., 2017). Moreover, the total number of vehicles in the NCP region increased from 38.7 million in 2013 to 60.3 million in 2017 (NBS, 2018), although high-emission motor vehicles are banned. Therefore, emissions from liquid fossil fuels are more important to eBC compared to solid fuels.

3.2 Contribution of regional transport to eBC

The 2–23 January, 2018 period was arbitrarily selected to explore the influence of regional transport on eBC loading in Xianghe using the WRF-Chem model. The simulated mass concentration of eBC was significantly correlated with the measured value ($R^2 = 0.61$, $p < 0.01$) as shown in Fig. S7. The estimated IOA was 0.72. This indicated that the formation process of eBC was captured by WRF-Chem. As shown in Fig. S8, six source regions were identified in the WRF-Chem model to quantify the contributions of local emissions and regional transport to observed eBC mass. The information on each source region is summarized in Table S2, and their contributions to observed eBC mass are shown in Fig. 5.

删除了: rush-hour traffic.... Although ...he peaks of eBC_{sf} were also showed two peaks appeared...ound to be in the same period with ...s eBC_{lf} However, they could be attributed tower affected by the...residential cooking activities ...n surrounding rural areas,...where solid fuels is ...re a commonly used source of household energy (Liu et al., 2016). Due to the increased planetary boundary layer height and wind speed (data sources see Text S1),Both...decreased eBC_{lf} and eBC_{sf} values were observed in the afternoon owing to the increases of planetary boundary layer height and wind speed...Fig. 32..., data sources see Text S2.... In contrast a ...he rapid decline in eBC_{lf} after 19:00, eBC_{sf} remained ...eristed at a high level until midnight. Meanwhile...oreover, the eBC_{sf}/eBC_{sf} ... fraction in eBC was also increased ...elevated towards to ...he night, indicating the ...hanced heating activities with the ...singe of...solid fuels during on

删除了: 3...shows ...mpares findings from variousome previous...studies regarding the ...BC source apportionment..., and their detailed information is summarized in Table S1. Because of the heavy traffic, IL...iquid fossil fuel source ...missions was an absolute...re major contributors to eBC mass at ...n urban area due to the heavy traffic.... However,...missions frombut the contribution of...solid fuel source... contribute more to eBC mass compared to liquid fossil fuels in enhances at ...ural area. This is attributed to, where...wood burning is commonly...sed as an energy source in households energy.... Furthermore...n addition, we can also find that ...he dominant eBC source in winter NCP has been ...hanged from past solid fuels to current liquid fossil fuels, even though uncertainty may be caused by the limited studies in the NCP... This change is probably attributed to the rigorous regulations that have been promulgated by the Chinese State Council in recent years,...of which t...he large-scale project of coal-to-gas switching has been...s considered as ...n effective way to ...f reducing atmospheric...pollutants (Qin et al., 2017). In addition...oreover, although high-emission motor vehicles are also banned, ...he total number of vehicles in the NCP region increased largely ...rom 38.7 million in 2013 to 60.3 million in 2017 (NBS, 2018), although high-emission motor vehicles are banned. Therefore, the ...missions from liquid fossil fuels source has become a...re more important contributor ...o eBC compared with the...o solid fuels source

删除了: period of3 January, 2018 period was arbitrarily...selected to explore the influence of regional contributions ...ransport on to ...BC loading inat...Xianghe using the WRF-Chem model. As shown in Fig. S5, t...he simulated BC ...ass concentration of eBC was correlated ...ignificantly correlated with the measured value ($R^2 = 0.61$, $p < 0.01$) as shown in Fig. S7,...and t...he estimated IOA was estimated to be ...72. This...indicated...that the BC ...ormation process of eBC was succeed ...aptured in catching ...y WRF-Chem. As shown in Fig. S8, To determine the impacts of local emission and regional transport on BC, we set up ...ix possible BC ...ource regions were identified in the WRF-Chem model to quantify the contributions of local emissions and regional transport to observed eBC mass.as part of the modelling exercise (Fig. S6),...and their location...he information on each source region is summarized in Table S2, and their contributions to observed eBC mass are shown in Fig. 5. The percent contributions from local emission and regional transport to BC mass are shown in Fig. 4. Although the contributions from different regions varied from day to day, the average BC mass contribution from ...

Local emissions (53%) contributed more to eBC mass compared to regional transport (47%). Furthermore, regional transport could be divided into 20% from Beijing, 5% from Tianjin, 11% from NCP, 9% from northern Hebei, and 2% from other regions. Fig. 6 shows the correlations between total eBC mass and the contributions of each source region. Local emission contributions were negatively correlated with eBC loading (Fig. 6a). This finding shows the increasing importance of regional transport at high eBC episode. Among the regional transport areas, the contributions of Tianjin and NCP exhibited a positive correlation with eBC loading (Fig. 6c and d), suggesting their important roles in eBC pollution at the sampling site. A high eBC loading episode was recorded on 12th-13th January and was taken as an example to explore the formation process of regional pollution (Fig. 7). On 11th of January before eBC pollution, strong north-westerly winds prevailed in the north of Xianghe. About 44% and 32% of the total eBC mass were contributed by Region 1 (local emissions) and Region 2 (Beijing), respectively. Afterwards, the winds turned to the southwest and passed over the NCP region on the 12th of January. The mass concentration of eBC increased sharply. Regional transport contributed to 83% of the total eBC mass, of which the NCP region accounted for 63% (Fig. 5). On the 13th of January, the winds switched towards the south over the NCP region but decreased near the sampling site. Therefore, the contribution of regional transport reduced to 66% of the total eBC mass with 40% from NCP region and 15% from Tianjin (Fig. 5). On 14th of January, the winds turned to the northwest, and the mass concentration of eBC decreased gradually. Finally, the high eBC pollution episode dissipated.

3.3 Chemical composition of EC-containing particles

The chemical compositions of EC-containing particles were determined using a SPAMS. A total of 454433 particles whose mass spectra had obvious carbon fragment ions (e.g., $m/z \pm 12, \pm 24, \pm 36, \pm 48, \pm 60$, and so on) were identified as EC-containing particles. Six particle categories including EC-OCsOx, EC-NaK, EC-KSOxNOx, EC-BB, pure-EC, and EC-others were classified based on their mass spectral feature. The average mass spectral pattern of each class is shown in Fig. 8, and the contribution of each class to the total EC-containing particles is summarized in Table 2.

The EC-OCsOx particles were characterized by obvious signals of organic carbon (OC) (e.g., $^{37}\text{C}_3\text{H}^+$, $^{39}\text{C}_3\text{H}_3^+$, $^{50}\text{C}_4\text{H}_2^+$, $^{27}\text{C}_2\text{H}_3^+$, $^{51}\text{C}_4\text{H}_3^+$, and $^{63}(\text{CH}_3)_2\text{NH}_2\text{OH}^+$) in the positive mass spectrum and strong

删除了: Local emissions (53%) contributed more to eBC mass compared to slightly higher than that from regional transport (47%). Furthermore, regional transport could be divided into including...20% from Beijing, 5% from Tianjin, 11% from NCP, 9% from northern Hebei, and 2% from other regions. Fig. 6 shows the correlations between total eBC mass and the contributions of each source region. Local emission contributions were Although the local emission was the largest contributor to BC mass on average for all the simulated days, its contribution exhibited a negatively correlated relation...with the...eBC loading (Fig. 65...). This finding shows the, indicating an...increasing importance of regional transport when the...t high eBC episode was occurred... Among the regional transport areas Actually... only BC...he contributions from...f Tianjin and NCP exhibited a positive correlation with increased as the...BC loading increased...(Fig. and d)...suggesting their that the south of Xianghe was an...important roles in pollution region to large...eBC pollution ma...

删除了: Taking the...ighest...eBC loading episode was recorded on 1... ..

删除了:

删除了: explain...xplore the formation process of regional transport...ollution (Fig. 76) ..

设置了格式: 上标 ..

设置了格式: 上标 ..

删除了: the high...BC loading episode...ollution, strong north-westerly winds prevailed in the north of Xianghe,...and a...bout 44% and 32% of the total eBC mass were contributed by local emission and Beijing as represented by...egion 1 (local emissions) and Region 2 (Beijing), respectively. Thereafter...fterwards, on 12 January, ..

设置了格式: 上标 ..

设置了格式: 上标 ..

删除了: loadings...increased sharply, ... with r...egional transport accounting for...ontributed to 83% of the total eBC mass, of which NCP region accounted for 63% (Fig. 54) ..

设置了格式: 上标 ..

删除了: T...e contribution of regional transport reduced to 66% of the total eBC mass with 40% from NCP region and 15% from Tianjin (Fig. 54)... ..

设置了格式: 上标 ..

删除了: after the high BC episode... the winds turned to the northwest, and then ..

删除了: BC coatings ..

删除了: BC...C-containing particles were coatings was...determined with...sing a SPAMS. A total of 454433 particles whose mass spectra had obvious BC...arbon fragment ions (e.g., $m/z \pm 12, \pm 24, \pm 36, \pm 48, \pm 60$, and so on) were identified as EB...-containing particles. Further, s...ix particle categories including EB...-OCsOx, EB...-NaK, EB...-KSOxNOx, EB...-BB, p...re-EB..., and EB...-others were classified based on their mass spectral features... The average mass spectral pattern of each class is shown in Fig. 87... and the contribution of each class to the total EB ..

删除了: B...-OCsOx particles were...characterized by obvious signals of organic carbon (OC) signals in the positive mass ..

5 sulphate signal ($^{97}\text{HSO}_4^-$) in the negative mass spectrum. This group exhibited the highest contribution to the total EC-containing particles (52%, Table 2), indicating that EC was mainly coated with OC and sulphate. The presences of $^{43}\text{C}_2\text{H}_3\text{O}^+$, a marker denoting the oxidized organics (Gunsch et al., 2018), and $^{97}\text{HSO}_4^-$ implied that EC-OCsOx underwent a certain degree of atmospheric aging process. Fig. 9 shows the number of fractions of each class of EC-containing particles at different ranges of eBC_{eff} and eBC_{sf} . The EC-OCsOx number fraction increased as eBC_{sf} increased. In contrast, it dropped when eBC_{eff} was higher than the value of the 75th percentile of eBC_{eff} . This indicated a greater impact of solid fuel source on EC-OCsOx at a high eBC loading environment compared to the liquid fossil fuel source. The diurnal variations in EC-OCsOx number fraction exhibited an upward trend at night after 19:00 (Fig. 10). This may be attributed to intensive domestic heating activities in the surrounding rural areas.

10 The EC-NaK particles presented strong signals of $^{23}\text{Na}^+$ and $^{39}\text{K}^+$ in the positive mass spectrum and less intense signals of $^{26}\text{CN}^-$, $^{46}\text{NO}_2^-$, $^{62}\text{NO}_3^-$, and $^{97}\text{HSO}_4^-$ in the negative mass spectrum. This group exhibited the second largest contribution to total EC-containing particles (24%, Table 2). Intense signals of carbon fragment ions (m/z 24, 36, 48, 60, and 72) were observed in the negative mass spectrum. This indicated that EC-NaK particles were freshly emitted. Additionally, larger signals were found for nitrate compared to sulphate in the negative mass spectrum. However, their signals were low. This finding was consistent with the motor vehicle emissions, which were shown to contain substantial nitrogen oxides (May et al., 2014). The number fraction of EC-NaK increased with an increase in eBC_{eff} but kept stable with eBC_{sf} as shown in Fig. 9. These results demonstrate that EC-NaK was likely associated with fresh traffic emissions than from solid fuels.

20 The EC-KSOxNOx particles exhibited strong $^{39}\text{K}^+$ signal in the positive mass spectrum and intense $^{46}\text{NO}_2^-$, $^{62}\text{NO}_3^-$, and $^{97}\text{HSO}_4^-$ signals in the negative mass spectrum. This group accounted for 17% of the total EC-containing particles (Table 2). The high signal intensities of nitrate and sulphate indicated that EC-KSOxNOx particles underwent substantive atmospheric aging processes. As shown in Fig. 10, the number fraction of the EC-KSOxNOx class was the only one that increased in the afternoon. This finding was consistent with the increase of ozone (O_3) as measured by an ultraviolet photometric Model 49i O_3 analyzer (Thermo Fisher Scientific, San Jose, CA, USA). This indicated that EC particles were more

删除了: signal in the negative mass spectrum. This group was exhibited the largest ... highest contribution to the total EC-containing particles, ... constituting ... 52%, of the total BC-containing particles (Table 2), indicating that EC... was mainly coated with OC and sulphate. The presences of $^{43}\text{C}_2\text{H}_3\text{O}^+$ (... a marker denoting the oxidized organics, ... (Gunsch et al., 2018), and $^{97}\text{HSO}_4^-$ implied... that EC...-OCsOx was ... underwent a certain degree of atmospheric aging processes. ... Fig. 9 shows the number of fractions of each class of EC-containing particles at different ranges of eBC_{eff} and eBC_{sf} . As shown in Fig. 8, ... the EC...-OCsOx number fraction increased as eBC_{sf} increased. In contrast, it dropped when eBC_{eff} was larger ... igher than the value of the 75th percentile of eBC_{eff} . This indicated... a greater impact of solid fuel source on EC...-OCsOx at a high eBC loading environment compared with ... o the liquid fossil fuel source. The diurnal variations in EC...-OCsOx number fraction exhibited an upward trend at night after 19:00 (Fig. 10). ... This which was... ay be attributed to the

删除了: B...-NaK particles presented exhibited ... strong signals of $^{23}\text{Na}^+$ and $^{39}\text{K}^+$ in the positive mass spectrum and less intense signals of $^{26}\text{CN}^-$, $^{46}\text{NO}_2^-$, $^{62}\text{NO}_3^-$, and $^{97}\text{HSO}_4^-$ in the negative mass spectrum. This group was ... exhibited the second largest contribution to accounting for 24% of ... total EC...-containing particles (24%, Table 2). Intense signals of carbon fragment ions (m/z 24, 36, 48, 60, and 72) were concentrated ... bserved in... the negative mass spectrum. This... indicated... that EC...-NaK particles were mainly ... freshly emitted. Meanwhile... dditionally, relatively higher... arger signals was ... ere found for nitrate than ... ompared to sulphate in the negative mass spectrum. However... although... their signals were low. This finding was... consistent with the motor vehicle emissions, which were shown to contain... substantial nitrogen oxides (May et al., 2014). Furthermore, t... the number fraction of EC...-NaK enhanced ... ncreased with an increase in... as... eBC_{eff} increased ... ut kept stable with eBC_{sf} as shown in (... Fig. 9). These results demonstrate that EC...-NaK was more ... ily associated with the... fresh traffic emissions than from relative to the ... old fuels emission

删除了: B...-KSOxNOx particles exhibited had a ... strong signal of $^{39}\text{K}^+$ signal in the positive mass spectrum and intense signals of $^{46}\text{NO}_2^-$, $^{62}\text{NO}_3^-$, and $^{97}\text{HSO}_4^-$ signals in the negative mass spectrum. This group comprised ... accounted for 17% of the total EC...-containing particles (Table 2). The high signal intensities of nitrate and sulphate indicated that EC...-KSOxNOx particles suffered ... nderwent substantive atmospheric... aging processes in the atmosphere... As shown in Fig. 10, t... e number fraction of the EC...-KSOxNOx class was the only class ... ne that increased in the afternoon, ... This finding which... was consistent with the increase of ozone (O_3), Fig. 9... as measured with ... y an ultraviolet photometric Model 49i O_3 analyzer (Thermo Fisher Scientific, San Jose, CA, USA). This indicated... that BC

likely to be coated with sulphate and nitrate in high oxidation environments. The strong $^{39}\text{K}^+$ ion signal in EC-KSOxNOx particles implied a partial influence of emissions from biomass burning (Bi et al., 2011).

The EC-BB particles were characterized by $^{39/41}\text{K}^+$ signals in the positive mass spectrum and $^{26}\text{CN}^-$, $^{46}\text{NO}_2^-$, and $^{97}\text{HSO}_4^-$ signals in the negative mass spectrum. It accounted for 6% of the total EC-containing particles as shown in Table 2. Several levoglucosan, $^{45}\text{CHO}_2^-$, $^{59}\text{C}_2\text{H}_3\text{O}_2^-$, and $^{73}\text{C}_3\text{H}_5\text{O}_2^-$ signals were also found in the negative mass spectrum. They suggested a typical biomass-burning feature. Intense signals of negative carbon ion spectrum (e.g., m/z -24, -36, and -48) and low signals of nitrate and sulphate indicated that EC-BB particles underwent low aging atmospheric processes.

The pure-EC particles were characterized by EC fragment ions (e.g., m/z ± 24 , ± 36 , ± 48 , ± 60 , and ± 72).

The low nitrate and sulphate ion signals in pure-EC indicated that they were freshly emitted. This group exhibited minor contributions to the total EC-containing particles (1%, Table 2). The particles of EC-others were characterized by some metallic signals (e.g., $^{40}\text{Ca}^+$, $^{56}\text{Fe}^+/\text{CaO}^+$, and $^{62}\text{FeO}^+$) and aromatic signatures (e.g., $^{51}\text{C}_4\text{H}_3^+$, $^{63}\text{C}_5\text{H}_3^+$, $^{77}\text{C}_6\text{H}_5^+$, and $^{91}\text{C}_7\text{H}_7^+$) in the positive mass spectrum and strong NO_2^- signal (m/z 46) in the negative mass spectrum. This indicated that EC-others underwent a certain degree of atmospheric aging processes and internally mixed with metals and aromatic compounds. This class accounted for 1% of the total EC-containing particles (Table 2).

3.4 Implications for radiative effect

Fig. 11 shows the eBC DRE variations as estimated by the SBDART model. The variations in eBC DRE were highly correlated with eBC burden on each day. Due to the decrease in radiative energy reaching the surface, eBC exhibited a DRE range of -1.9 to -27.9 W m^{-2} with an average of $-13.6 \pm 7.0 \text{ W m}^{-2}$ at the ES, indicating a cooling effect. In contrast, eBC exhibited a DRE range of $+0.6$ to $+20.8 \text{ W m}^{-2}$ with an average of $+4.4 \pm 3.0 \text{ W m}^{-2}$ at the TOA, indicating a net energy gain and warm effect. This was attributed to the strong BC light absorption property that can impede the back scattered radiation reaching the TOA. The eBC DRE at the TOA in this study was comparable to the value over the NCP region ($+6$ to $+8 \text{ W m}^{-2}$, Li et al., 2016).

The difference between eBC DRE at the TOA and ES gave an atmospheric DRE (a net atmospheric absorption) of $+18.0 \pm 9.6 \text{ W m}^{-2}$. This corresponded to a heating rate of 0.5 K day^{-1} . The eBC DRE in

删除了: easier ... to be coated with sulphate and nitrate in the more...igh oxidation environments. The strong $^{39}\text{K}^+$ ion signal in the ...B...-KSOxNOx particles may ...pliedy...a partial influence of emissions from biomass ...urning emissions

删除了: B...-BB particles were contributed only 6% to total BC-containing particles (Table 2), and it was ...haracterized by signals of $^{39/41}\text{K}^+$ signals in the positive mass spectrum and $^{26}\text{CN}^-$, $^{46}\text{NO}_2^-$, and $^{97}\text{HSO}_4^-$ signals in the negative mass spectrum. It accounted for 6% of the total EC-containing particles as shown in Table 2. Several levoglucosan signals of $^{45}\text{CHO}_2^-$, $^{59}\text{C}_2\text{H}_3\text{O}_2^-$, and $^{73}\text{C}_3\text{H}_5\text{O}_2^-$ signals were also existed ...ound in the negative mass spectrum. They,...suggesting ...uggested a typical biomass-burning characterization...eature. Intense signals of negative carbon ion spectrum of BC... (e.g., m/z -24, -36, and -48) and relatively ...ow signals of nitrate and sulphate indicated that EB...-BB particles underwent low aging atmospheric processes were less aged in the atmosphere... Due to the intensive heating activities, this class had an increased contribution to total BC-containing particles at night (Fig. 9).

删除了: P...re-EB... particles were was mainly...characterized by EB... fragment ions (e.g., m/z ± 24 , ± 36 , ± 48 , ± 60 , and ± 72). The IL...w ion signals of ...itrate and sulphate ion signals in pure-EC indicated that Pure-BC was... they were freshly emitted. This group exhibited minor contributions minor (1%, Table 2)... to the total EB...-containing particles (1%, Table 2). The particles of EB...-others were ...ere characterized by some metallic signals (e.g., $^{40}\text{Ca}^+$, $^{56}\text{Fe}^+/\text{CaO}^+$, and $^{62}\text{FeO}^+$) and aromatic signatures (e.g., $^{51}\text{C}_4\text{H}_3^+$, $^{63}\text{C}_5\text{H}_3^+$, $^{77}\text{C}_6\text{H}_5^+$, and $^{91}\text{C}_7\text{H}_7^+$) in the positive mass spectrum and strong signal of $^{46}\text{NO}_2^-$ signal (m/z 46) in the negative mass spectrum. This indicates... that this type of B...-C-others underwent particles experienced...a certain degree of atmospheric aging processes in the atmosphere ...nd internally mixed with metals and aromatic compounds. This class accounted for only...1% of the total EB

删除了: forcing effect...RE was ...ere highly associated ...related with eBC burden in ...n each day. As shown in Fig. 10, d...ue to reduction ...he decrease in radiative energy reaching the surface, through absorbing incoming sunlight, ...BC had ...xhibited a DREcooling effect...range of -1.9 to -27.9 W m^{-2} with an average of $13.6 \pm 7.0 \text{ W m}^{-2}$ at the ES, ranging from ...indicating a cooling effect -1.9 to -27.9 W m^{-2} . In contrast, eBC had ...xhibited a DRE range of $+0.6$ to $+20.8 \text{ W m}^{-2}$ with an average warm effect ...f $+4.4 \pm 3.0 \text{ W m}^{-2}$ at the TOA, varying from $+0.6$ to $+20.8 \text{ W m}^{-2}$, ...ndicating a net energy gain and warm effect. This was partly

删除了: F...at the TOA and the...ES gave the ...n atmospheric forcing ...RE (a net atmospheric absorption) of $+18.0 \pm 9.6 \text{ W m}^{-2}$ This which ...corresponded to a heating rate of 0.5 K day^{-1} . The eBC DRE F

the atmosphere accounted for 86% of the total aerosol DRE (+21.0 W m⁻²), suggesting that eBC exhibited a significant impact on perturbing the Earth-atmosphere radiative balance. The atmospheric heating in conjunction with the surface reduction in solar flux may aggravate the low-level inversion. This can lead to a slowdown of thermal convection and in turn reduce the cloud formation process (Chou et al., 2002).

5 Compared to previous DRE obtained from the SBDART model, the atmospheric DRE derived by eBC values in this study (+18.0 ± 9.6 W m⁻²) was comparable to that of South China (+17.0 W m⁻², Huang et al., 2011) but was lower than that of Northwest China (+16.6 to +108.8 W m⁻², Zhao et al., 2019). In addition to the varying BC burden in different areas, the BC measurement techniques used in different studies may also contribute to the differences in BC DRE calculations.

10 As shown in Fig. 11c and d, the mean eBC DRE caused by the sources of liquid fossil fuels (solid fuels) was -7.0 W m⁻² (-5.4 W m⁻²) at the ES and +2.1 W m⁻² (+1.7 W m⁻²) at the TOA. It produced an atmospheric DRE of +9.1 W m⁻² (+7.1 W m⁻²). Due to a stronger eBC DRF, the average heating rate (0.3 K day⁻¹) of the atmosphere caused by liquid fossil fuel sources was 33% more than that of solid fuels (0.2 K day⁻¹). Although larger eBC DRE was found for liquid fossil fuel sources, its atmospheric DRE
15 generated per unit eBC mass concentration (3.6 (W m⁻²) (μg m⁻³)⁻¹) was 81% smaller compared to that of solid fuels (6.5 (W m⁻²) (μg m⁻³)⁻¹). This implies that reduction in eBC from solid fuel emissions may be a more effective way to mitigate regional warming in the NCP region, and eBC from motor vehicle emissions should also be controlled.

4 Conclusions

20 The sources, coating composition, and radiative effects of BC were investigated during winter in the last year of the APPCAP at a regional site in the NCP. Based on the source-specific AAEs (AAE_{lf} = 1.3 and AAE_{sf} = 2.8), about 69% of eBC was contributed by liquid fossil fuel sources while the rest 31% was contributed by solid fuel sources using a multi-wavelength optical method. Both eBC_{lf} and eBC_{sf} exhibited peaks at 08:00 and 19:00. Due to rigorous regulations, the dominant eBC source in winter NCP
25 may be changed from past solid fuels to current liquid fossil fuels. The WRF-Chem model showed that local emissions (53%) were the largest contributors to eBC loading on average, followed by Beijing (20%), Tianjin (5%), NCP (11%), northern Hebei (9%), and other regions (2%).

删除了: F
删除了: has

删除了: ,
删除了: ing
删除了: ing

删除了: process of

删除了: 0
删除了: F
删除了: source
删除了: ,
删除了: ing
删除了: forcing
删除了: (0.3 K day⁻¹)

删除了: source
删除了: F
删除了: forcing
删除了: with
删除了: the
删除了: source

删除了: of
删除了: BC

删除了: though
删除了: emission

删除了: s
删除了: is

删除了: needed to
删除了: produced

删除了: n aethalometer model
删除了: The

删除了: both
删除了: showed two

删除了: but with different causes
删除了: s

删除了: was

Among the six classes of EC-containing particles, EC-OCsOx was the largest contributor (52%). The presence of $^{43}\text{C}_2\text{H}_3\text{O}^+$ and $^{97}\text{HSO}_4^-$ in this particle implied that it underwent a certain degree of atmospheric aging processes. Solid fuel sources exhibited a greater impact on EC-OCsOx at a high eBC loading environment compared to liquid fossil fuels. EC-NaK was the second largest contributor to total EC-containing particles (24%). This class was associated with fresh traffic emissions than with solid fuels. EC-KSOxNOx accounted for 17% of the total EC-containing particles. This class was partially influenced by biomass-burning emissions and underwent substantive atmospheric aging processes. The classes of EC-BB, pure-EC, and EC-others exhibited minor contributions to the total EC-containing particles (1-6%).

删除了: Based on the mass spectral characteristics... BC coated with OC and sulphate (B...C-OCsOx)...was the largest contributor (52%) to the measured BC-containing particles... The presences...of $^{43}\text{C}_2\text{H}_3\text{O}^+$ and $^{97}\text{HSO}_4^-$ in this particle implied...that BC-OCsOx was...t underwent a certain degree of atmospheric aging processes. The s...olid fuel sources exhibited had...a greater impact on EB...-OCsOx at a high eBC loading environment compared with ...othe...liquid fossil fuel source.... BC coated with Na and K (B...C-NaK)...was the second largest contributor to total EB...-containing particles (24%).... Tand t...is class was more likely ...associated with the ...fresh traffic emissions than with relative to the...solid fuel emission.... BC coated with K, sulphate, and nitrate (B...C-KSOxNOx)...accounted for 17% of the total EB...-containing particles. This class was partially influenced by biomass-burning emissions and suffered ...nderwent substantive atmospheric...aging processes in the atmosphere... The rest ...lasses of EB...-BB, pP...re-EB..., and EB...-others contributed ...hibited minor contributions to the total EB...-containing particles (1 ...

The SBDART model showed that eBC induced a cooling effect of -13.6 W m^{-2} at the ES and a warming effect of $+4.4 \text{ W m}^{-2}$ at the TOA. The difference between eBC DRE at the TOA and ES gave the atmospheric forcing of $+18.0 \pm 9.6 \text{ W m}^{-2}$. This produced a heating rate of 0.5 K day^{-1} on average. The atmospheric DRE of eBC had a contribution of 86% to the forcing caused by total aerosols in the atmosphere. This suggested that BC exhibited a significant impact on perturbing the Earth-atmosphere radiative balance. From the eBC source perspective, the atmospheric eBC DRE was higher for liquid fossil fuel source than solid fuel source. However, the atmospheric DRE generated per unit eBC mass concentration was larger for solid fuel sources. This indicates that a reduction in solid fuel eBC may be an effective way of mitigating regional warming in the NCP.

删除了: s...that eBC can... induced a cooling effect of -13.6 W m^{-2} at the ES and a warming effect of $+4.4 \text{ W m}^{-2}$ at the TOA. The difference between eBC DRE...at the TOA and ES gave the atmospheric forcing of $+18.0 \pm 9.6 \text{ W m}^{-2}$ This which can ...roduced a heating rate of 0.5 K day^{-1} on average. The atmospheric forcing ...RE of eBC had a contribution ofed...86% to the forcing caused by total aerosols in the atmosphere....This suggested...that BC exhibitedhad...a significant impact on perturbing the Earth-atmosphere radiative balance. From the perspective of ...BC source perspectives... the atmospheric forcing of ...BC DRE was higher for liquid fossil fuel source than the ...olid fuel source. However,...the atmospheric forcing ...RE generated per unit eBC mass concentration was larger for solid fuel sources. This indicates that a reduction of ...n solid fuel eBC may be an more ...ffective way to further...f mitigatingthe...regional warming in the NCP compared with BC that emitted from motor vehicles ...

Data availability. The data presented in this study are available at the Zenodo data archive <https://doi.org/10.5281/zenodo.3923612>.

Supplement. The supplement related to this article is available online.

Author contributions. QW and JC designed the campaign. QW and WR carried out the field measurements. YZ and WR conducted the source experiments. QW, LL, JZ, and JY analyzed the data. QW drafted the paper. All the authors reviewed and commented on the paper.

Competing interests. The authors declare that they have no conflict of interest.

Acknowledgments. This study was supported by the Strategic Priority Research Program of Chinese Academy of Sciences (XDB40000000), the Natural Science Foundation of China (21661132005), the West Light Foundation of the Chinese Academy of Sciences (XAB2018B03), and the Youth Innovation Promotion Association of the Chinese Academy of Sciences (2019402). The authors are grateful to the staff from Xianghe Atmospheric Integrated Observatory for their assistance with field sampling.

删除了: 3

删除了: 2

References:

- An, Z., Huang, R.-J., Zhang, R., Tie, X., Li, G., Cao, J., Zhou, W., Shi, Z., Han, Y., Gu, Z., and Ji, Y.: Severe haze in northern China: A synergy of anthropogenic emissions and atmospheric processes, *Proc. Natl. Acad. Sci. U. S. A.*, 116, 8657–8666, <https://doi.org/10.1073/pnas.1900125116>, 2019.
- 10 Arndt, J., Sciare, J., Mallet, M., Roberts, G. C., Marchand, N., Sartelet, K., Sellegri, K., Dulac, F., Healy, R. M., and Wenger, J. C.: Sources and mixing state of summertime background aerosol in the north-western Mediterranean basin, *Atmos. Chem. Phys.*, 17, 6975–7001, <https://doi.org/10.5194/acp-17-6975-2017>, 2017.
- 15 Bi, X., Zhang, G., Li, L., Wang, X., Li, M., Sheng, G., Fu, J., and Zhou, Z.: Mixing state of biomass burning particles by single particle aerosol mass spectrometer in the urban area of PRD, China, *Atmos. Environ.*, 45, 3447–3453, <https://doi.org/10.1016/j.atmosenv.2011.03.034>, 2011.
- Bond, T. C., Doherty, S. J., Fahey, D. W., Forster, P. M., Berntsen, T., DeAngelo, B. J., Flanner, M. G., Ghan, S., Kaercher, B., Koch, D., Kinne, S., Kondo, Y., Quinn, P. K., Sarofim, M. C., Schultz, M. G., Schulz, M., Venkataraman, C., Zhang, H., Zhang, S., Bellouin, N., Guttikunda, S. K., Hopke, P.
- 20 K., Jacobson, M. Z., Kaiser, J. W., Klimont, Z., Lohmann, U., Schwarz, J. P., Shindell, D., Storelvmo, T., Warren, S. G., and Zender, C. S.: Bounding the role of black carbon in the climate system: A scientific assessment, *J. Geophys. Res.-Atmos.*, 118, 5380–5552, <https://doi.org/10.1002/jgrd.50171>, 2013.
- Boiyo, R., Kumar, K. R., Zhao, T., and Guo, J.: A 10-year record of aerosol optical properties and radiative forcing over three environmentally distinct AERONET sites in Kenya, East Africa, *J. Geophys. Res.-Atmos.*, 124, 1596–1617, <https://doi.org/10.1029/2018JD029461>, 2019.

- Briggs, N. L., and Long, C. M.: Critical review of black carbon and elemental carbon source apportionment in Europe and the United States, *Atmos. Environ.*, 144, 409–427, <https://doi.org/10.1016/j.atmosenv.2016.09.002>, 2016.
- Cheng, Y., Lee, S. C., Ho, K. F., Chow, J. C., Watson, J. G., Louie, P. K. K., Cao, J. J., and Hai, X.: Chemically-specified on-road PM_{2.5} motor vehicle emission factors in Hong Kong, *Sci. Total Environ.*, 408, 1621–1627, <https://doi.org/10.1016/j.scitotenv.2009.11.061>, 2010.
- Chou, M. D., Chan, P. K., and Wang, M. H.: Aerosol radiative forcing derived from SeaWiFS-retrieved aerosol optical properties, *J. Atmos. Sci.*, 59, 748–757, [https://doi.org/10.1175/1520-0469\(2002\)059<0748:Arfdfs>2.0.Co;2](https://doi.org/10.1175/1520-0469(2002)059<0748:Arfdfs>2.0.Co;2), 2002.
- Ding, A. J., Huang, X., Nie, W., Sun, J. N., Kerminen, V. M., Petäjä, T., Su, H., Cheng, Y. F., Yang, X. Q., Wang, M. H., Chi, X. G., Wang, J. P., Virkkula, A., Guo, W. D., Yuan, J., Wang, S. Y., Zhang, R. J., Wu, Y. F., Song, Y., Zhu, T., Zilitinkevich, S., Kulmala, M., and Fu, C. B.: Enhanced haze pollution by black carbon in megacities in China, *Geophys. Res. Lett.*, 43, 2873–2879, <https://doi.org/10.1002/2016GL067745>, 2016.
- Drinovec, L., Močnik, G., Zotter, P., Prévôt, A. S. H., Ruckstuhl, C., Coz, E., Rupakheti, M., Sciare, J., Müller, T., Wiedensohler, A., and Hansen, A. D. A.: The "dual-spot" Aethalometer: an improved measurement of aerosol black carbon with real-time loading compensation, *Atmos. Meas. Tech.*, 8, 1965–1979, <https://doi.org/10.5194/amt-8-1965-2015>, 2015.
- Eriksson, A. C., Wittbom, C., Roldin, P., Sporre, M., Öström, E., Nilsson, P., Martinsson, J., Rissler, J., Nordin, E. Z., Svenningsson, B., Pagels, J., and Swietlicki, E.: Diesel soot aging in urban plumes within hours under cold dark and humid conditions, *Sci. Rep.*, 7, 12364, <https://doi.org/10.1038/s41598-017-12433-0>, 2017.
- Fierce, L., Bond, T. C., Bauer, S. E., Mena, F., and Riemer, N.: Black carbon absorption at the global scale is affected by particle-scale diversity in composition, *Nat. Commun.*, 7, 12361, <https://doi.org/10.1038/ncomms12361>, 2016.
- Gunsch, M. J., May, N. W., Wen, M., Bottenus, C. L. H., Gardner, D. J., VanReken, T. M., Bertman, S. B., Hopke, P. K., Ault, A. P., and Pratt, K. A.: Ubiquitous influence of wildfire emissions and

删除了: Boucher, O., Randall, D., Artaxo, P., Bretherton, C., Feingold, G., Forster, P., Kerminen, V.-M., Kondo, Y., Liao, H., Lohmann, U., Rasch, P., Satheesh, S. K., Sherwood, S., Stevens, B., and Zhang, X. Y.: Clouds and Aerosols, in: *Climate Change 2013: The Physical Science Basis, Contribution of Working Group I to the Fifth Assessment Report of the Intergovernmental Panel on Climate Change*, edited by: Stocker, T. F., Qin, D., Plattner, G.-K., Tignor, M., Allen, S. K., Boschung, J., Nauels, A., Xia, Y., Bex, V., and Midgley, P. M., Cambridge University Press, Cambridge, United Kingdom and New York, USA, 2013.

secondary organic aerosol on summertime atmospheric aerosol in the forested Great Lakes region, *Atmos. Chem. Phys.*, 18, 3701–3715, <https://doi.org/10.5194/acp-18-3701-2018>, 2018.

5 Heald, C. L., Ridley, D. A., Kroll, J. H., Barrett, S. R. H., Cady-Pereira, K. E., Alvarado, M. J. and Holmes, C. D.: Contrasting the direct radiative effect and direct radiative forcing of aerosols, *Atmos. Chem. Phys.*, 14(11), 5513–5527, <https://doi.org/10.5194/acp-14-5513-2014>, 2014.

Hess, M., Koepke, P., and Schult, I.: Optical Properties of Aerosols and Clouds: The Software Package OPAC, *Bulletin of the American Meteorological Society*, 79, 831–844, 10.1175/1520-0477(1998)079<0831:OPOAAC>2.0.CO;2, 1998.

10 Huang, X. F., Gao, R. S., Schwarz, J. P., He, L. Y., Fahey, D. W., Watts, L. A., McComiskey, A., Cooper, O. R., Sun, T. L., Zeng, L. W., Hu, M. and Zhang, Y. H.: Black carbon measurements in the Pearl River Delta region of China, , 116, 1–10, doi:10.1029/2010JD014933, 2011.

Li, K., Liao, H., Mao, Y. and Ridley, D. A.: Source sector and region contributions to concentration and direct radiative forcing of black carbon in China, *Atmos. Environ.*, 124, 351–366, <https://doi.org/10.1016/j.atmosenv.2015.06.014>, 2016.

15 Kalogridis, A. C., Vratolis, S., Liakakou, E., Gerasopoulos, E., Mihalopoulos, N., and Eleftheriadis, K.: Assessment of wood burning versus fossil fuel contribution to wintertime black carbon and carbon monoxide concentrations in Athens, Greece, *Atmos. Chem. Phys.*, 18, 10219–10236, <https://doi.org/10.5194/acp-18-10219-2018>, 2018.

20 Kim, J.-H., Kim, S.-W., Ogren, J. A., Sheridan, P. J., Yoon, S.-C., Sharma, S. and Lin, N.-H.: Multiple scattering correction factor estimation for aethalometer aerosol absorption coefficient measurement, *Aerosol Sci. Technol.*, 53(2), 160–171, <https://doi.org/10.1080/02786826.2018.1555368>, 2019.

Kopp, R. E., and Mauzerall, D. L.: Assessing the climatic benefits of black carbon mitigation, *Proc. Natl. Acad. Sci. U. S. A.*, 107, 11703–11708, <https://doi.org/10.1073/pnas.0909605107>, 2010.

25 Laskin, A., Laskin, J., and Nizkorodov, S. A.: Chemistry of atmospheric brown carbon, *Chem. Rev.*, 115, 4335–4382, <https://doi.org/10.1021/cr5006167>, 2015.

Li, B., Gasser, T., Ciais, P., Piao, S., Tao, S., Balkanski, Y., Hauglustaine, D., Boisier, J.-P., Chen, Z., Huang, M., Li, L. Z., Li, Y., Liu, H., Liu, J., Peng, S., Shen, Z., Sun, Z., Wang, R., Wang, T., Yin,

- G., Yin, Y., Zeng, H., Zeng, Z., and Zhou, F.: The contribution of China's emissions to global climate forcing, *Nature*, 531, 357–361, <https://doi.org/10.1038/nature17165>, 2016.
- Li, G., Bei, N., Tie, X., and Molina, L. T.: Aerosol effects on the photochemistry in Mexico City during MCMA- 2006/MILAGRO campaign, *Atmos. Chem. Phys.*, 11, 5169–5182, <https://doi.org/10.5194/acp-11-5169-2011>, 2011.
- Li, L., Wang, Q., Zhang, X., She, Y., Zhou, J., Chen, Y., Wang, P., Liu, S., Zhang, T., Dai, W., Han, Y., and Cao, J.: Characteristics of single atmospheric particles in a heavily polluted urban area of China: size distributions and mixing states, *Environ. Sci. Pollut. Res.*, 26, 11730–11742, <https://doi.org/10.1007/s11356-019-04579-3>, 2019.
- Liou, K. N.: An introduction to atmospheric radiation, (2nd ed.p 583), New York: Academic press, Elsevier Science, 2002.
- Liu, D., Whitehead, J., Alfarra, M. R., Reyes-Villegas, E., Spracklen, Dominick V., Reddington, Carly L., Kong, S., Williams, Paul I., Ting, Y.-C., Haslett, S., Taylor, Jonathan W., Flynn, Michael J., Morgan, William T., McFiggans, G., Coe, H., and Allan, James D.: Black-carbon absorption enhancement in the atmosphere determined by particle mixing state, *Nat. Geosci.*, 10, 184–188, <https://doi.org/10.1038/ngeo2901>, 2017.
- Liu, J., Mauzerall, D. L., Chen, Q., Zhang, Q., Song, Y., Peng, W., Klimont, Z., Qiu, X., Zhang, S., Hu, M., Lin, W., Smith, K. R., and Zhu, T.: Air pollutant emissions from Chinese households: A major and underappreciated ambient pollution source, *Proc. Natl. Acad. Sci. U. S. A.*, 113, 7756–7761, <https://doi.org/10.1073/pnas.1604537113>, 2016.
- May, A. A., Nguyen, N. T., Presto, A. A., Gordon, T. D., Lipsky, E. M., Karve, M., Gutierrez, A., Robertson, W. H., Zhang, M., Brandow, C., Chang, O., Chen, S., Cicero-Fernandez, P., Dinkins, L., Fuentes, M., Huang, S.-M., Ling, R., Long, J., Maddox, C., Massetti, J., McCauley, E., Miguel, A., Na, K., Ong, R., Pang, Y., Rieger, P., Sax, T., Truong, T., Vo, T., Chattopadhyay, S., Maldonado, H., Maricq, M. M., and Robinson, A. L.: Gas- and particle-phase primary emissions from in-use, on-road gasoline and diesel vehicles, *Atmos. Environ.*, 88, 247–260, <https://doi.org/10.1016/j.atmosenv.2014.01.046>, 2014.

NBS (National Bureau of Statistics): China Statistical Yearbook 2018, China Statistics Press, Beijing, available at: <http://www.stats.gov.cn/tjsj/ndsj/> (last access: October 2019), 2018

5 [Qin, Y., Wagner, F., Scovronick, N., Peng, W., Yang, J., Zhu, T., Smith, K. R. and Mauzerall, D. L.: Air quality, health, and climate implications of China's synthetic natural gas development, *Proc. Natl. Acad. Sci.*, 114\(19\), 4887–4892, <https://doi.org/10.1073/pnas.1703167114>, 2017.](#)

Rajesh, T. A., and Ramachandran, S.: Black carbon aerosols over urban and high altitude remote regions: Characteristics and radiative implications, *Atmos. Environ.*, 194, 110–122, <https://doi.org/10.1016/j.atmosenv.2018.09.023>, 2018.

10 Raju, M. P., Safai, P. D., Vijayakumar, K., Devara, P. C. S., Naidu, C. V., Rao, P. S. P., and Pandithurai, G.: Atmospheric abundances of black carbon aerosols and their radiative impact over an urban and a rural site in SW India, *Atmos. Environ.*, 125, 429–436, <https://doi.org/10.1016/j.atmosenv.2015.09.023>, 2016.

15 Ricchiuzzi, P., Yang, S. R., Gautier, C., and Sowle, D.: SBDART: A research and teaching software tool for plane-parallel radiative transfer in the Earth's atmosphere, *Bull. Amer. Meteorol. Soc.*, 79, 2101–2114, [https://doi.org/10.1175/1520-0477\(1998\)079<2101:Sarats>2.0.Co;2](https://doi.org/10.1175/1520-0477(1998)079<2101:Sarats>2.0.Co;2), 1998.

Sandradewi, J., Prévôt, A. S. H., Szidat, S., Perron, N., Alfarra, M. R., Lanz, V. A., Weingartner, E., and Baltensperger, U.: Using aerosol light absorption measurements for the quantitative determination of wood burning and traffic emission contributions to particulate matter, *Environ. Sci. Technol.*, 42, 3316–3323, <https://doi.org/10.1021/es702253m>, 2008.

20 [Sun, J. Z., Zhi, G. R., Jin, W. J., Chen, Y. J., Shen, G. F., Tian, C. G., Zhang, Y. Z., Zong, Z., Cheng, M. M., Zhang, X. M., Zhang, Y., Liu, C. Y., Lu, J. K., Wang, H. Z., Xiang, J. M., Tong, L. T., and Zhang, X.: Emission factors of organic carbon and elemental carbon for residential coal and biomass fuels in China—A new database for 39 fuel-stove combinations, *Atmos. Environ.*, 190, 241–248, <https://doi.org/10.1016/j.atmosenv.2018.07.032>, 2018.](#)

25 Tian, J., Chow, J. C., Cao, J., Han, Y., Ni, H., Chen, L. W. A., Wang, X., Huang, R., Moosmüller, H., and Watson, J. G.: A biomass combustion chamber: design, evaluation, and a case study of wheat straw combustion emission tests, *Aerosol Air Qual. Res.*, 15, 2104–2114, <https://doi.org/10.4209/aaqr.2015.03.0167>, 2015.

删除了: Singh, A., Srivastava, R., Rastogi, N., and Singh, D.: Absorbing and scattering aerosols over the source region of biomass burning emissions: Implications in the assessment of optical and radiative properties, *Atmos. Environ.*, 127, 61–68, <https://doi.org/10.1016/j.atmosenv.2015.12.029>, 2016.

- Vignati, E., Karl, M., Krol, M., Wilson, J., Stier, P., and Cavalli, F.: Sources of uncertainties in modelling black carbon at the global scale, *Atmos. Chem. Phys.*, 10, 2595–2611, <https://doi.org/10.5194/acp-10-2595-2010>, 2010.
- Wang, Q., Huang, R. J., Cao, J., Han, Y., Wang, G., Li, G., Wang, Y., Dai, W., Zhang, R., and Zhou, Y.:
5 Mixing state of black carbon aerosol in a heavily polluted urban area of China: implications for light absorption enhancement, *Aerosol Sci. Technol.*, 48, 689–697, <https://doi.org/10.1080/02786826.2014.917758>, 2014.
- Wang, Q., Cao, J., Han, Y., Tian, J., Zhu, C., Zhang, Y., Zhang, N., Shen, Z., Ni, H., Zhao, S., and Wu, J.: Sources and physicochemical characteristics of black carbon aerosol from the southeastern
10 Tibetan Plateau: internal mixing enhances light absorption, *Atmos. Chem. Phys.*, 18, 4639–4656, [10.5194/acp-18-4639-2018](https://doi.org/10.5194/acp-18-4639-2018), 2018.
- Wang, Q., Liu, S., Li, N., Dai, W., Wu, Y., Tian, J., Zhou, Y., Wang, M., Ho, S. S. H., Chen, Y., Zhang, R., Zhao, S., Zhu, C., Han, Y., Tie, X., and Cao, J.: Impacts of short-term mitigation measures on PM_{2.5} and radiative effects: a case study at a regional background site near Beijing, China, *Atmos.
15 Chem. Phys.*, 19, 1881–1899, <https://doi.org/10.5194/acp-19-1881-2019>, 2019a.
- Wang, Q., Ye, J., Wang, Y., Zhang, T., Ran, W., Wu, Y., Tian, J., Li, L., Zhou, Y., Hang Ho, S. S., Dang, B., Zhang, Q., Zhang, R., Chen, Y., Zhu, C., and Cao, J.: Wintertime Optical Properties of Primary and Secondary Brown Carbon at a Regional Site in the North China Plain, *Environ. Sci. Technol.*,
53, 12389–12397, <https://doi.org/10.1021/acs.est.9b03406>, 2019b.
- 20 Yang, M., Howell, S. G., Zhuang, J., and Huebert, B. J.: Attribution of aerosol light absorption to black carbon, brown carbon, and dust in China – interpretations of atmospheric measurements during EAST-AIRE, *Atmos. Chem. Phys.*, 9, 2035–2050, <https://doi.org/10.5194/acp-9-2035-2009>, 2009.
- Zhang, G., Bi, X., He, J., Chen, D., Chan, L. Y., Xie, G., Wang, X., Sheng, G., Fu, J., and Zhou, Z.:
Variation of secondary coatings associated with elemental carbon by single particle analysis, *Atmos.
25 Environ.*, 92, 162–170, <https://doi.org/10.1016/j.atmosenv.2014.04.018>, 2014.
- Zhang, Y., Forrister, H., Liu, J., Dibb, J., Anderson, B., Schwarz, J. P., Perring, A. E., Jimenez, J. L., Campuzano-Jost, P., Wang, Y., Nenes, A., and Weber, R. J.: Top-of-atmosphere radiative forcing

删除了: Tian, J., Wang, Q., Ni, H., Wang, M., Zhou, Y., Han, Y., Shen, Z., Pongpiachan, S., Zhang, N., Zhao, Z., Zhang, Q., Zhang, Y., Long, X., and Cao, J.: Emission characteristics of primary brown carbon absorption from biomass and coal burning: development of an optical emission inventory for China, *J. Geophys. Res.-Atmos.*, 124, 1879–1893, [10.1029/2018JD029352](https://doi.org/10.1029/2018JD029352), 2019.

删除了: a

删除了: Wang, Q., Cao, J., Han, Y., Tian, J., Zhang, Y., Pongpiachan, S., Zhang, Y., Li, L., Niu, X., Shen, Z., Zhao, Z., Tipmanee, D., Bunsomboonsakul, S., Chen, Y., and Sun, J.: Enhanced light absorption due to the mixing state of black carbon in fresh biomass burning emissions, *Atmospheric Environment*, 180, 184–191, <https://doi.org/10.1016/j.atmosenv.2018.02.049>, 2018b.

- affected by brown carbon in the upper troposphere, *Nat. Geosci.*, 10, 486–489, <https://doi.org/10.1038/ngeo2960>, 2017.
- Zhang, Y.-L., Schnelle-Kreis, J., Abbaszade, G., Zimmermann, R., Zotter, P., Shen, R.-r., Schäfer, K., Shao, L., Prévôt, A. S. H., and Szidat, S.: Source apportionment of elemental carbon in Beijing, China: insights from radiocarbon and organic marker measurements, *Environ. Sci. Technol.*, 49, 8408–8415, <https://doi.org/10.1021/acs.est.5b01944>, 2015.
- Zhao, S., Tie, X., Cao, J., Li, N., Li, G., Zhang, Q., Zhu, C., Long, X., Li, J., Feng, T., and Su, X.: Seasonal variation and four-year trend of black carbon in the Mid-west China: The analysis of the ambient measurement and WRF-Chem modeling, *Atmos. Environ.*, 123, 430–439, <https://doi.org/10.1016/j.atmosenv.2015.05.008>, 2015.
- Zhang, Q., Zheng, Y., Tong, D., Shao, M., Wang, S., Zhang, Y., Xu, X., Wang, J., He, H., Liu, W., Ding, Y., Lei, Y., Li, J., Wang, Z., Zhang, X., Wang, Y., Cheng, J., Liu, Y., Shi, Q., Yan, L., Geng, G., Hong, C., Li, M., Liu, F., Zheng, B., Cao, J., Ding, A., Gao, J., Fu, Q., Huo, J., Liu, B., Liu, Z., Yang, F., He, K., and Hao, J.: Drivers of improved PM_{2.5} air quality in China from 2013 to 2017, *Proc. Natl. Acad. Sci. U. S. A.*, 116, 24463, <https://doi.org/10.1073/pnas.1907956116>, 2019.
- Zheng, H., Kong, S., Wu, F., Cheng, Y., Niu, Z., Zheng, S., Yang, G., Yao, L., Yan, Q., Wu, J., Zheng, M., Chen, N., Xu, K., Yan, Y., Liu, D., Zhao, D., Zhao, T., Bai, Y., Li, S., and Qi, S.: Intra-regional transport of black carbon between the south edge of the North China Plain and central China during winter haze episodes, *Atmos. Chem. Phys.*, 19, 4499–4516, <https://doi.org/10.5194/acp-19-4499-2019>, 2019.
- Zhao, S., Yu, Y., Yin, D., Yu, Z., Dong, L., Mao, Z., He, J., Yang, J., Li, P. and Qin, D.: Concentrations, optical and radiative properties of carbonaceous aerosols over urban Lanzhou, a typical valley city: Results from in-situ observations and numerical model, *Atmos. Environ.*, 213, 470–484, <https://doi.org/10.1016/j.atmosenv.2019.06.046>, 2019.
- Zotter, P., Herich, H., Gysel, M., El-Haddad, I., Zhang, Y., Močnik, G., Hüglin, C., Baltensperger, U., Szidat, S., and Prévôt, A. S. H.: Evaluation of the absorption Ångström exponents for traffic and wood burning in the Aethalometer-based source apportionment using radiocarbon measurements of

删除了: Zhang, Y. L., El-Haddad, I., Huang, R. J., Ho, K. F., Cao, J. J., Han, Y., Zotter, P., Bozzetti, C., Daellenbach, K. R., Slowik, J. G., Salazar, G., Prévôt, A. S. H., and Szidat, S.: Large contribution of fossil fuel derived secondary organic carbon to water soluble organic aerosols in winter haze in China, *Atmos. Chem. Phys.*, 18, 4005–4017, <https://doi.org/10.5194/acp-18-4005-2018>, 2018.

ambient aerosol, *Atmos. Chem. Phys.*, 17, 4229–4249, <https://doi.org/10.5194/acp-17-4229-2017>, 2017.